Definition of the IEA 15-Megawatt Offshore Reference Wind Turbine

Gaertner, Evan; Rinker, Jennifer; Sethuraman, Latha; Zahle, Frederik; Anderson, Benjamin; Barter, Garrett; Abbas, Nikhar; Meng, Fanzhong; Bortolotti, Pietro; Skrzypinski, Witold

Total number of authors:
17

Publication date:
2020

Document Version
Publisher's PDF, also known as Version of record

March 2020

IEA Wind TCP Task 37

Definition of the IEA Wind 15-Megawatt Offshore Reference Wind Turbine

Technical Report

Definition of the IEA 15-Megawatt Offshore Reference Wind

Evan Gaertner[1], Jennifer Rinker[2], Latha Sethuraman[1], Frederik Zahle[2], Benjamin Anderson[1], Garrett Barter[1], Nikhar Abbas[1], Fanzhong Meng[2], Pietro Bortolotti[1], Witold Skrzypinski[2], George Scott[1], Roland Feil[1], Henrik Bredmose[2], Katherine Dykes[2], Matt Shields[1], Christopher Allen[3], and Anthony Viselli[3]

1 National Renewable Energy Laboratory
2 Technical University of Denmark
3 University of Maine

Suggested Citation
Gaertner, Evan, Jennifer Rinker, Latha Sethuraman, Frederik Zahle, Benjamin Anderson, Garrett Barter, Nikhar Abbas, Fanzhong Meng, Pietro Bortolotti, Witold Skrzypinski, George Scott, Roland Feil, Henrik Bredmose, Katherine Dykes, Matt Shields, Christopher Allen, and Anthony Viselli. 2020. *Definition of the IEA 15-Megawatt Offshore Reference Wind*. Golden, CO: National Renewable Energy Laboratory. NREL/TP-5000-75698. https://www.nrel.gov/docs/fy20osti/75698.pdf

NREL is a national laboratory of the U.S. Department of Energy
Office of Energy Efficiency & Renewable Energy
Operated by the Alliance for Sustainable Energy, LLC

This report is available at no cost from the National Renewable Energy Laboratory (NREL) at www.nrel.gov/publications.

Contract No. DE-AC36-08GO28308

Technical Report
NREL/TP-5000-75698
March 2020

National Renewable Energy Laboratory
15013 Denver West Parkway
Golden, CO 80401
303-275-3000 • www.nrel.gov

NOTICE

This work was authored in part by the National Renewable Energy Laboratory, operated by Alliance for Sustainable Energy, LLC, for the U.S. Department of Energy (DOE) under Contract No. DE-AC36-08GO28308. Funding provided by U.S. Department of Energy Office of Energy Efficiency and Renewable Energy Wind and Water Technologies Office. The views expressed herein do not necessarily represent the views of the DOE or the U.S. Government.

Acknowledgements

Staff from the National Renewable Energy Laboratory (NREL) and the Technical University of Denmark (DTU) collaborated closely, via the International Energy Agency (IEA) Wind Task 37 on Systems Engineering in Wind Energy, to design the reference turbine described in this report. The authors from the University of Maine (UMaine) leveraged their expertise and resources to contribute the floating platform semisubmersible design. To better capture the individual contributions, and as a resource for future inquiries, the following table lists the roles and responsibilities for all of the authors involved.

Name	Institution	Contribution
Evan Gaertner	NREL	Primary design engineer who led the blade, tower, and monopile design
Jennifer Rinker	DTU	HAWC2 lead, design load basis, controller tuning
Latha Sethuraman	NREL	Designer of permanent-magnet direct-drive generator, drivetrain, bedplate, nacelle, and other subsystems
Frederik Zahle	DTU	Bend-twist coupling contribution, rotor and blade design review
Benjamin Anderson	NREL	Created nacelle CAD model and performed drivetrain and bedplate analysis
Garrett Barter	NREL	Project principal investigator
Nikhar Abbas	NREL	Reference OpenSource Controller lead and tuning
Fanzhong Meng	DTU	Controller lead and tuning
Pietro Bortolotti	NREL	Blade design support
Witold Skrzypiński	DTU	Tool development for blade design
George Scott	NREL	Drivetrain design support
Roland Feil	NREL	Detailed blade structural analysis
Henrik Bredmose	DTU	COREWIND principal investigator
Katherine Dykes	DTU	General support
Matt Shields	NREL	Monopile and transition piece design support, report editing
Christopher Allen	UMaine	Lead semisubmersible design engineer
Anthony Viselli	UMaine	Semisubmersible principal investigator

Beyond IEA Wind facilitated collaboration between NREL, DTU, and UMaine, the larger networks of individual staff members and the IEA Wind Task 37 effort were leveraged to ensure that the design represented a conservative estimate of industry capabilities. These industry contacts gave invaluable information to calibrate our design assumptions and input values. Without their input, the 15-MW reference turbine would not be nearly as professional of a design or as useful to the broader community. In no particular order, we extend our thanks to the following companies and individuals:

- General Electric: Anna Diedrichkeit, Albert Fiass, Vanita Mani, Priyan Subramanian, David Torrey, Yogen Utturkar
- EDF Renewables: Julien Simon
- Senvion: Fabian Vorpahl
- Sintef: Karl Merz
- Atkins: Ikpoto Udoh
- NREL: Walt Musial, Jason Jonkman, Nicole Mendoza
- Sandia National Laboratories: Ernesto Camarena.

The work at NREL was sponsored by the U.S. Department of Energy Office of Energy Efficiency and Renewable Energy Wind Energy Technologies Office under the guidance of program manager, Patrick Gilman. The research at DTU received funding from the European Union's H2020 Program under Grant Agreement no. 815083 - COREWIND.

Nomenclature

Acronyms	
3D	three-dimensional
BECAS	BEam Cross section Analysis Software
DLC	design load case
DTU	Technical University of Denmark
HAWTOpt2	Horizontal Axis Wind Turbine Optimization 2nd generation
HAWC2	Horizontal Axis Wind turbine simulation Code 2nd generation
IEC	International Electrotechnical Commission
IEA	International Energy Agency
metocean	meteorological ocean
NREL	National Renewable Energy Laboratory
NdFeB	neodymium
PSD	power spectral density
PI	proportional integral
ROSCO	Reference OpenSource Controller
RMS	root mean squared
SRB	spherical roller bearing
SST	shear stress transport
TDO	tapered double outer
TSR	tip-speed ratio
UMaine	University of Maine
WindPACT	Wind Partnership for Advanced Component Technology
WISDEM®	Wind-Plant Integrated System Design Engineering Model
WP	work package
Units	
A	ampere
h	hour
Hz	hertz
kg	kilogram
m	meter
min	minute
N (kgm/s^2)	Newton
rad	radian
rpm	revolutions per minute
P	period
Pa (N/m^2)	pascal
s	second
t	metric tonne
T	tesla
V	volt
W	watt
Prefixes	
m	milli
k	kilo
M	mega
G	giga

Executive Summary

Overview and Motivation

Reference wind turbines serve multiple roles within the wind community and have therefore grown in importance in recent years. First, they serve as open benchmarks that are defined with publicly available design parameters to be used as baselines for studies that explore new technologies or design methodologies. Second, as an open design, reference wind turbines enable collaboration between industry and external researchers. Finally, reference wind turbines offer an entry point and educational platform for newcomers to wind energy to understand fundamental design elements and system trade-offs.

For fixed-bottom offshore wind energy, the average turbine size for European deployment in 2018 was 6.8 MW [1], and GE will launch its 12-MW Haliade-X offshore turbine to the market in 2021 with a rotor diameter of 218 m and direct-drive configuration. To be relevant now and in the coming years, a new reference wind turbine should leap ahead of the current generation of industry wind turbines, but cannot leap so far that aggressive technology innovations are required. Therefore, a reference wind turbine above 10 MW [2], yet below 20 MW [3], is needed, that continues on the same growth trend as the GE Haliade-X using a similar drivetrain configuration and specific power.

This report describes a 15-megawatt (MW) offshore wind turbine with a fixed-bottom monopile support structure. This reference wind turbine is a Class IB direct-drive machine, with a rotor diameter of 240 meters (m) and a hub height of 150 m. An overview of the design is presented in Figure ES-1 and Table ES-1. The design reflects a joint effort between the National Renewable Energy Laboratory (NREL), sponsored by the U.S. Department of Energy, and the Technical University of Denmark (DTU), sponsored by the European Union's H2020 Program, through the second work package of International Energy Agency (IEA) Wind Task 37 on Wind Energy Systems Engineering: Integrated RD&D. A forthcoming report will detail a semisubmersible floating support structure developed by the University of Maine (UMaine).

Blade and Rotor Properties

Top level rotor configuration decisions were informed by discussions with industry partners, on what would be technically feasible for the next generation of wind turbines. The blade design was driven by the selection of 240 m as the rotor diameter and a maximum tip speed of 95 meters per second (m/s). A fairly traditional structural configuration was selected, comprising of two main load-carrying, carbon-reinforced spars, connected by two shear webs, with reinforcement along the trailing and leading edge and foam fillers. The DTU FFA-W3 series of airfoils were used due to their publicly available polars and geometries. The blade chord, twist, airfoil positions, tip speed ratio, and spar cap thickness were selected through a design optimization study. Table ES-2 summarized key features of the blades, including a design power coefficient, C_P, of 0.489 and 65 metric tons (t) of blade mass.

Tower and Monopile Properties

The tower and monopile were designed as an isotropic steel tube. Frequency considerations constrained much of the design in that the first tower-monopile mode, 0.17 hertz (Hz), lies between the 1P and 3P blade passing frequencies for all wind speeds. This is also sufficient to avoid the range of highest energy ocean wave frequencies for a generic East Coast site (0.10 Hz to 0.13 Hz). The tower height was chosen such that the hub height reaches 150 m, allowing for 30 m of ground (water surface) clearance with up to 120-m blades. The monopile foundation has a 10-m outer diameter, which pushes the limits of current manufacturing and installation technology, and a thickness profile that varies from 55 millimeters (mm) in the pile to 44 mm at the transition piece.

Nacelle and Drivetrain Properties

The 15-MW reference wind turbine uses a direct-drive layout with a permanent-magnet, synchronous, radial flux outer-rotor generator in a simple and compact nacelle layout. Figure ES-2a shows a simple direct-drive nacelle layout with an outer-rotor permanent-magnet generator. The assembly consists of a hub shaft supporting the turbine

Table ES-1. Key Parameters for the IEA Wind 15-MW Turbine

Parameter	Units	Value
Power rating	MW	15
Turbine class	-	IEC Class 1B
Specific rating	W/m^2	332
Rotor orientation	-	Upwind
Number of blades	-	3
Control	-	Variable speed
		Collective pitch
Cut-in wind speed	m/s	3
Rated wind speed	m/s	10.59
Cut-out wind speed	m/s	25
Design tip-speed ratio	-	9 0
Minimum rotor speed	rpm	5.0
Maximum rotor speed	rpm	7.56
Maximum tip speed	m/s	95
Rotor diameter	m	240
Airfoil series	-	FFA-W3
Hub height	m	150
Hub diameter	m	7.94
Hub overhang	m	11.35
Rotor precone angle	deg	-4.0
Blade prebend	m	4
Blade mass	t	65
Drivetrain	-	Direct drive
Shaft tilt angle	deg	6
Rotor nacelle assembly mass	t	1,017
Transition piece height	m	15
Monopile embedment depth	m	45
Monopile base diameter	m	10
Tower mass	t	860
Monopile mass	t	1,318

deg	degrees	rpm	revolutions per minute
m	meters	t	metric tons
m/s	meters per second	W/m^2	watts per square meter

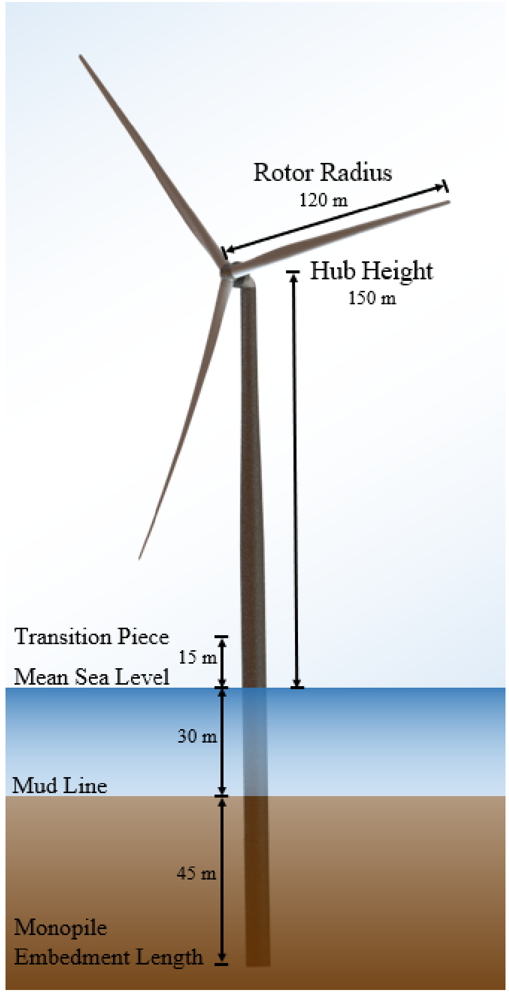

Figure ES-1. The IEA Wind 15-MW reference wind turbine

and generator rotors on two main bearings housed on a stationary turret that is cantilevered from the bedplate. The hub is a simple spherical shell, with cutouts for the blades and the flange. The main shaft has a hollow cylindrical cross section, with a constant wall thickness and a tilt angle of 6°. The main shaft, along with the rotor, is supported by two main bearings. Both these main bearings have rotating outer raceways and fixed inner raceways. The outer raceways and bearing housing are accommodated by a turret held by the bedplate. The entire weight of the turbine rotor, generator rotor, and hub loads are transmitted by the main shaft to the turret via the bearings. The bedplate is a hollow, elliptically curved, cantilever beam with circular cross sections. The yaw system bearings are double-row, angular, contact ball bearings.

The generator construction features an external rotor radial flux topology machine with a surface-mounted permanent magnet (shown in Figure ES-2b). The outer rotor layout facilitates a simple and rugged structure, easy manufacturing, short end windings, and better heat transfer between windings and teeth than the inner rotor configuration. The stator design features fractional, slot-layout, double-layer concentrated coils, which maximize the fundamental winding factor.

Load Analysis

This work assumes a generic U.S. East Coast site with a wind speed described by a Weibull distribution with a mean velocity of approximately 8.65 m/s and a shape parameter of 2.12. At this mean wind speed, the corresponding significant wave height is approximately 1.4 m, with a peak spectral period of 7.9 seconds (s). The fixed-bottom

Table ES-2. Blade Properties

Description	Value	Units
Blade length	117	m
Root diameter	5.20	m
Root cylinder length	2.34	m
Max chord	5.77	m
Max chord spanwise position	27.2	m
Tip prebend	4.00	m
Precone	4.00	deg
Blade mass	65,250	kg
Blade center of mass	26.8	m
Design tip-speed ratio	9.00	-
First flapwise natural frequency	0.555	Hz
First edgewise natural frequency	0.642	Hz
Design C_P	0.489	-
Design C_T	0.799	-
Annual energy production	77.4	GWh

deg	degrees	kg	kilograms
GWh	gigawatt-hours	m	meters
Hz	Hertz		

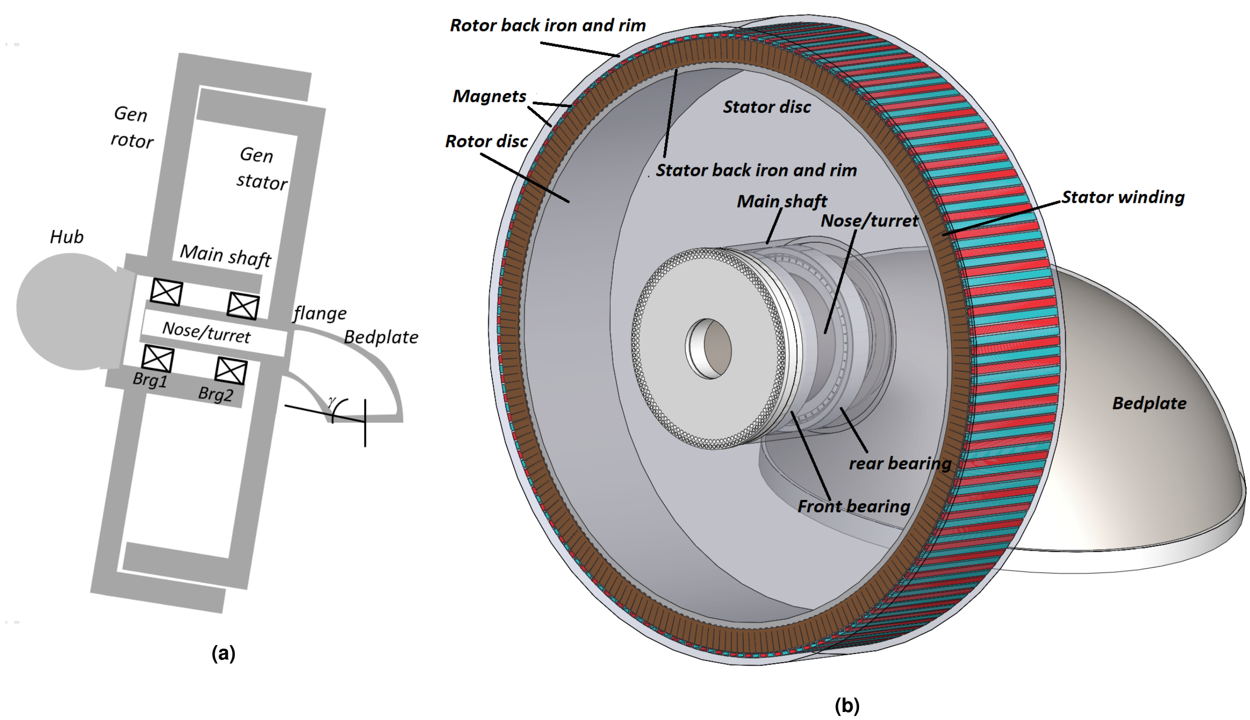

Figure ES-2. A sketch and CAD model of the nacelle layout of the 15-MW direct-drive wind turbine. Not to scale and some structural details omitted. Blades (not shown), hub, shaft, and generator rotor rotate.

monopile support presented in this report is designed around a water depth of 30 m.

An International Electrotechnical Commission design load case [4] analysis study was conducted to determine the worst-case ultimate loading on key design constraining components. Yaw-misaligned parked conditions with extreme wind speeds and extreme coherent gust with a direction change result in the worst-case loading for this design. The worst-case out-of-plane tip deflection is 22.8 m, leaving more than sufficient tower clearance, with an unbent blade tip-to-tower clearance of 30.0 m. This margin suggests that the blade design is conservative and further aeroelastic optimization could potentially improve the aerodynamic performance or cost of energy while still remaining within recommended safety margins. A full fatigue analysis of this blade was not conducted, which could potentially be an issue for the edgewise blade bending moments for very large blades.

Availability

To foster further collaboration, the reference turbine design is available for use by the broader wind energy community in input files that support a variety of analysis tools, including OpenFAST, HAWC2, the Wind-Plant Integrated System Design & Engineering Model (WISDEM), and HawtOpt2. These files are hosted on GitHub at github.com/IEAWindTask37/IEA-15-240-RWT, with the intent that the community will contribute back to the effort by submitting their design variants for inclusion in the repository.

Contents

List of Figures

List of Tables

1 Introduction

1.1 The Role of Reference Wind Turbines

Reference wind turbines serve multiple roles within the wind community and have therefore grown in importance in recent years. First, they serve as open benchmarks that are defined with publicly available design parameters to be used as baselines for studies that explore new technologies or design methodologies. Traditionally, reference wind turbines have been realistic, but not fully optimized, designs so that they can be updated and improved upon by the active wind energy community. Second, as an open design, reference wind turbines enable collaboration between industry and external researchers. By using a reference turbine, industry can protect its intellectual property yet still explore advanced technology development with outsiders. Finally, reference wind turbines offer an entry point and educational platform for newcomers to wind energy to understand fundamental design elements and system trade-offs.

The history of reference wind turbines begins in the early 2000s with the National Renewable Energy Laboratory (NREL) Wind Partnership for Advanced Component Technology (WindPACT) turbine series, which includes 0.75-, 1.5-, and 3-megawatt (MW) turbines [5]. Their use, however, was restricted to national laboratories in the United States. The first widely adopted reference turbine by the larger international community was the NREL 5-MW turbine [6], which is still used by many researchers today. More recently, the Technical University of Denmark (DTU) developed a 10-MW turbine for offshore wind applications [7]. These two turbines have been supplemented by other turbines, such as an 8-MW turbine in the European Union FP7 project LEANWIND [8], the Sandia National Laboratories' 100-meter (m)-blade studies [9], and a conceptual study of a 20-MW turbine in the INNWIND project [3]. Most recently, the IEA Wind Task 37, which coordinated this effort, also released modernized 3.35-MW land-based and 10-MW offshore reference turbines [2]. These designs have been released quickly on the heels of one another as the industry has rapidly increased the power rating and size of its product lines. For fixed-bottom offshore wind energy, the average turbine size for European deployment in 2018 was 6.8 MW [1], and GE will launch its 12-MW Haliade-X offshore turbine to the market in 2021 with a rotor diameter of 218 m and direct-drive configuration.

To be relevant now and in the coming years, a new reference wind turbine must leap ahead of the current generation of industry wind turbines, but cannot leap so far that aggressive technology innovations are required. The current slate of reference wind turbine designs cannot fully meet the needs of the research community and industry to advance the state of the art in blade scaling, floating foundation design, wind farm control, logistic studies, and many other topics. Therefore, a reference wind turbine above 10 MW, yet below 20 MW, is needed that continues on the same growth trend as the GE Haliade-X using a similar drivetrain configuration and specific power.

This is the motivation for the design effort of this IEA Wind 15-MW reference wind turbine described in this report. This reference wind turbine, Figure 1-1, is a Class IB direct-drive machine, with a rotor diameter of 240 m and a hub height of 150 m. The design reflects a joint effort between NREL, sponsored by the U.S. Department of Energy, and DTU, sponsored by the European Union's H2020 Program, through the second work package of IEA Wind Task 37 on Wind Energy Systems Engineering: Integrated RD&D. This report describes an offshore fixed-bottom monopile support structure, with a forthcoming report to detail a semisubmersible floating support structure developed in collaboration with the University of Maine (UMaine).

1.2 Overall Turbine Parameters

The overall parameters for the turbine are stated in Table 1-1. The table also shows the data for the DTU 10-MW reference wind turbine [7] for comparison.

1.3 Design Tools and Methodologies

The IEA Wind 15-MW reference turbine was jointly designed by NREL, DTU, and UMaine. The analysis and design tools that were leveraged as part of this effort are listed in Table 1-2. These model names will appear frequently in the discussion of the design in the sections to come.

Table 1-1. Key Parameters for the IEA Wind 15-MW Turbine, As Compared to the DTU 10-MW Turbine

Parameter	Units	DTU 10-MW Turbine	IEA Wind 15-MW Turbine
Power rating	MW	10	15
Turbine class	-	IEC Class 1B	IEC Class 1B
Specific rating	W/m^2	401	332
Rotor orientation	-	Upwind	Upwind
Number of blades	-	3	3
Control	-	Variable speed	Variable speed
	-	Collective pitch	Collective pitch
Cut-in wind speed	m/s	4	3
Rated wind speed	m/s	11.4	10.59
Cut-out wind speed	m/s	25	25
Rotor diameter	m	178.3	240
Airfoil series	-	FFA-W3	FFA-W3
Hub height	m	119	150
Hub diameter	m	5.6	7.94
Hub overhang	m	7.1	11.35
Drivetrain	-	Medium speed	Low speed
	-	Multiple-stage gearbox	Direct drive
Design tip-speed ratio	-	7.5	9.0
Minimum rotor speed	rpm	6.0	5.0
Maximum rotor speed	rpm	9.6	7.56
Maximum tip speed	m/s	90	95
Gearbox ratio	-	50	—
Shaft tilt angle	deg	5	6
Rotor precone angle	deg	-2.5	-4.0
Blade prebend	m	3.332	4
Blade mass	t	41	65
Rotor nacelle assembly mass	t	674	1,017
Tower mass	t	987	860
Tower base diameter	m	8	10
Transition piece height	m	10	15
Monopile embedment depth	m	42.6	45
Monopile base diameter	m	9	10
Monopile mass	t	2,044	1,318

deg	degrees	rpm	revolutions per minute
m	meters	t	metric tons
m/s	meters per second	W/m^2	watts per square meter
MW	megawatts		

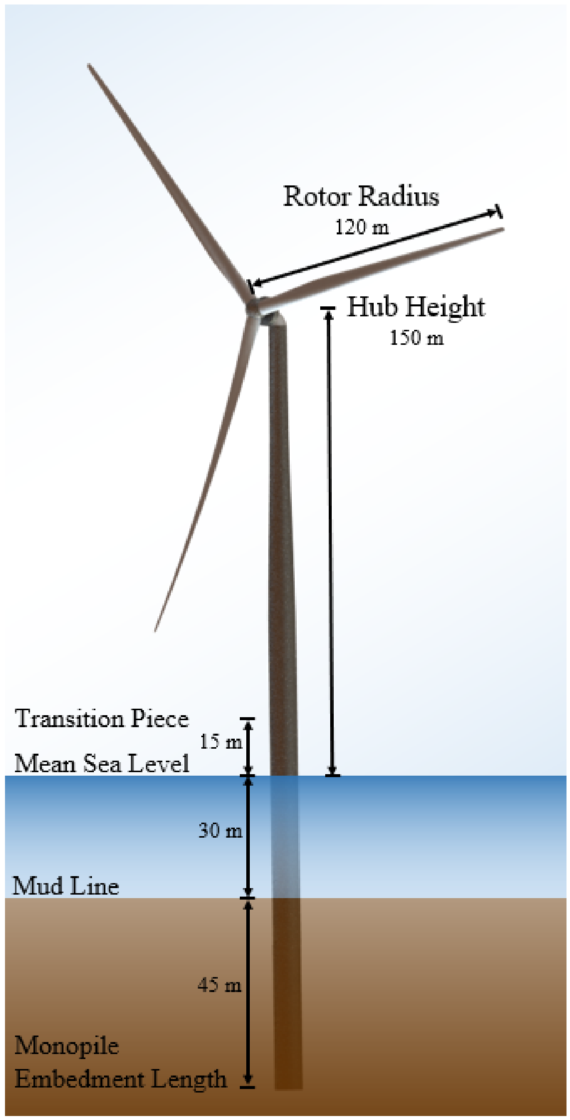

Figure 1-1. The IEA Wind 15-MW reference wind turbine

Table 1-2. Models Used for Design and Analysis of the IEA Wind 15-MW Reference Wind Turbine

Role	NREL Tool Chain	DTU Tool Chain
System Design	WISDEM [10], [11] CCBlade [14] RotorSE [15] DrivetrainSE TowerSE	HAWTOpt2 [12], [13]
Preprocessors	PreComp [16] BModes [18]	BECAS [17]
Aeroelastic Analysis	OpenFAST [19], [20]	HAWC2 [21] HAWCStab2 [22]

Most of the design was conducted within the Wind-Plant Integrated System Design & Engineering Model (WISDEM®), which is a family of models that are generally simplified and quasi-static to enable rapid design optimization at a limited number of design points. WISDEM is built on top of National Atmospheric and Space Administrations's OpenMDAO library, which drives the optimization and serves as the glue code between different models [23]. Conceptual designs were verified and enriched with more complete load and performance analysis using the nonlinear transient models of OpenFAST, HAWC2, and HAWCStab2. The results of these higher-fidelity simulations were used to update the design variable bounds and constraint values within WISDEM, and the process was iterated.

1.4 Model Availability

The reference turbine design is available for use by the broader wind energy community in input files that support a variety of analysis tools, including OpenFAST, HAWC2, WISDEM, and HawtOpt2. Additionally, the data depicted in graphs and tables in this report are also available electronically, in Microsoft Excel format, instead of writing them out as appendices. These files are hosted on GitHub at:

- github.com/IEAWindTask37/IEA-15-240-RWT
- github.com/IEAWindTask37/IEA-15-240-RWT/blob/master/Documentation.

The open-source availability of the IEA Wind 15-MW reference wind turbine is intended to encourage the community to contribute back to the effort by submitting their design variants for inclusion into the repository and further use by others.

1.5 Meteorological Ocean Environment

As a generic reference turbine, the design is intended to apply to many different offshore locations. However, the analysis of ultimate loads and the design of the substructure depend on the particular wind, wave, and soil profiles. The work of Stewart et al. [24] provides a general yet specific enough meteorological ocean (metocean) environment to execute the analysis and design. This work assumes a generic U.S. East Coast site, with detailed wind and wave probability distributions found in the repository documentation listing described in the previous subsection. As a quick summary, the wind speed is described as a Weibull distribution with parameters [9.767, 2.12], which gives a mean velocity of approximately 8.65 meters per second (m/s). At this mean wind speed, the corresponding significant wave height is approximately 1.4 m, with a peak spectral period of 7.9 seconds (s). The fixed-bottom monopile support presented in this report is designed around a water depth of 30 m.

2 Blade Properties

The blade length of this IEA Wind 15-MW reference turbine is 117 m with a root diameter of 5.2 m and a maximum chord of 5.77 m at approximately 20% span. The overall blade mass is around 65 metric tons (t) and is designed to achieve a power coefficient, C_P, of 0.489. A top-down and edge view of the blade are shown in Figure 2-1 and a more complete statistical breakdown is listed in Table 2-1.

Figure 2-1. View from the suction side (top) and trailing edge (bottom) of the offshore wind turbine blade

Table 2-1. Blade Properties

Description	Value	Units
Blade length	117	m
Root diameter	5.20	m
Root cylinder length	2.34	m
Max chord	5.77	m
Max chord spanwise position	27.2	m
Tip prebend	4.00	m
Precone	4.00	deg
Blade mass	65,250	kg
Blade center of mass	26.8	m
Design tip-speed ratio	9.00	-
First flapwise natural frequency	0.555	Hz
First edgewise natural frequency	0.642	Hz
Design C_P	0.489	-
Design C_T	0.799	-
Annual energy production	77.4	GWh

deg	degrees	kg	kilograms
GWh	gigawatt-hours	m	meters
Hz	Hertz		

2.1 Blade Aerodynamic Properties

The DTU FFA-W3 series of airfoils for use in the blade design. These are publicly available and well-documented airfoils that were also used in the IEA Wind/DTU 10-MW offshore reference wind turbine and are shown in Figure 2-2.

The airfoil data for each of the FFA-W3 airfoils was generated at a Reynolds number of $Re = 10^7$. To compute the aerodynamic coefficients in the range of $-32°$ to $32°$, we used the two-dimensional incompressible Navier-Stokes solver, EllipSys2D [25–27]. The meshes were generated using HypGrid2D [28], with a 512-by-256-cell radial grid. Simulations assumed fully turbulent and freely transitioning boundary layers, based on the $k-\omega$ shear stress transport (SST) turbulence model [29] and the Drela-Giles transition model [30], assuming a freestream turbulence intensity of 0.1%. We performed a 360° extrapolation using AirfoilPreppy, but three-dimensional (3D) corrections were not applied to the polars because the spanwise distribution of relative thickness was a free design variable. A Du-Selig [31] stall delay 3D correction was applied to the polar data for the OpenFAST model of the final design. Figure 2-3 shows the aerodynamic characteristics of the airfoils used on the blade. Tabular data of airfoil shapes and performance polars are provided in the parallel spreadsheet documentation.

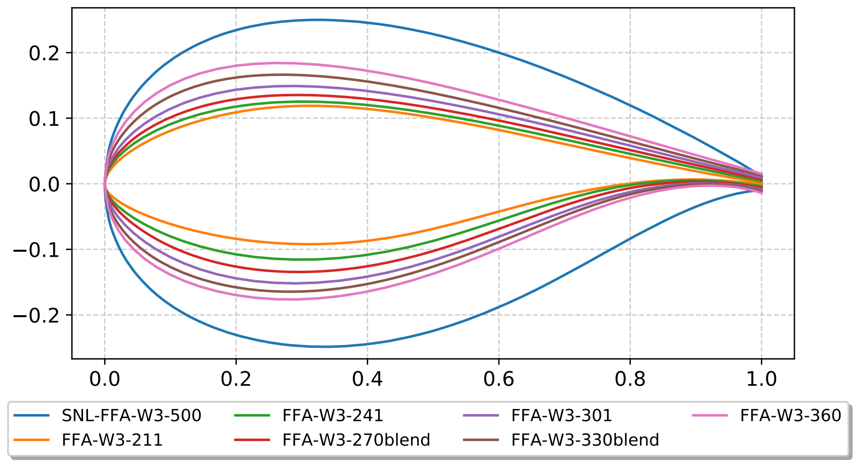

Figure 2-2. DTU FFA-W3 airfoil family used in the IEA Wind 15-MW blade design

The blade planform design variables are plotted in Figure 2-4. The aerodynamic center of the airfoils is used for the blade pitch axis. There are a number of aerodynamic design characteristics that are worth noting. The transition from a cylinder cross section to the thickest 50% airfoil occurs between 2.34 m to 17.55 m or 2%–15% of the span, with the maximum chord of 5.77 m at 27.2 m of span (23.3%). This is shown in the chord and relative thickness profiles in Figure 2-4a–b. With such a large blade radius, the design was heavily driven by the tip deflection loading and tower clearance constraint. The twist profile in Figure 2-4c shows some unloading at the blade tip, which sheds some energy production to mitigate the strongest thrust loads at the most flexible part of the blade. This behavior will be evident again in the rotor performance plots in Section 3. The blade was designed with a significant prebend away from the tower to provide additional tip clearance, with 4 m separating the tip chordline from the root (Figure 2-4d). When axially stacking the airfoils to generate the lofted blade shape, the cant angle from prebend curvature is not considered. More prebend would have given further margin, reducing stiffness requirements, but the value was limited to 4 m based on blade molding and other manufacturing challenges, as communicated by industry. Advanced manufacturing techniques may enable greater blade prebend in the future, but this is a reasonable constraint at this time.

2.2 Blade Structural Properties

The lofted blade shape is shown in Figure 2-5 and an internal structural layout at 70% span is shown in Figure 2-6, with additional spanwise locations in Appendix A. The structural layout of the blade is fairly traditional, comprising two main load-carrying spars placed on a straight line connecting the root and the tip, along with reinforcement along the trailing and leading edges. One of these spar caps is placed on the airfoil pressure side and the other on the suction side. These spar caps are made out of carbon fiber to provide as much stiffness with as little weight as possible. The blade has two shear webs that connect the pressure side and suction side, attached to the main spars, extending from a 10% to 95% span; shown in Figure 2-6 as the vertical members. Leading and trailing edge reinforcements are also added using uniaxial glass fiber to provide additional edgewise stiffness. Foam filler panels were added between the leading-edge and trailing-edge reinforcement and the spar caps, on both the pressure side and suction side.

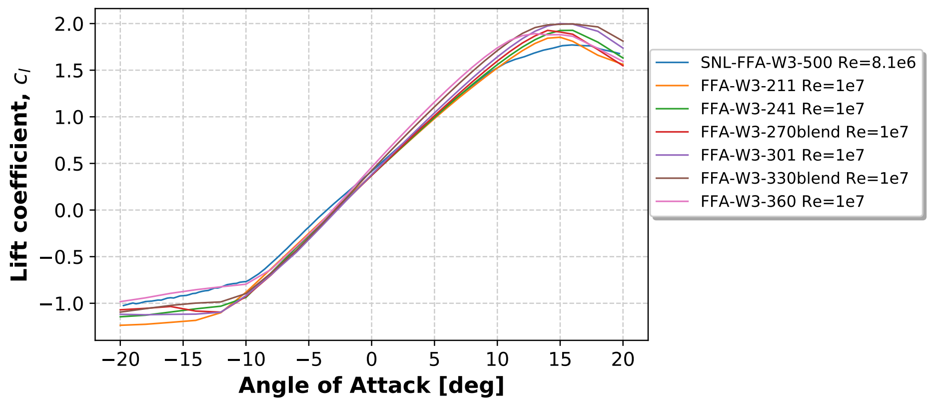

(a) Airfoil lift coefficients

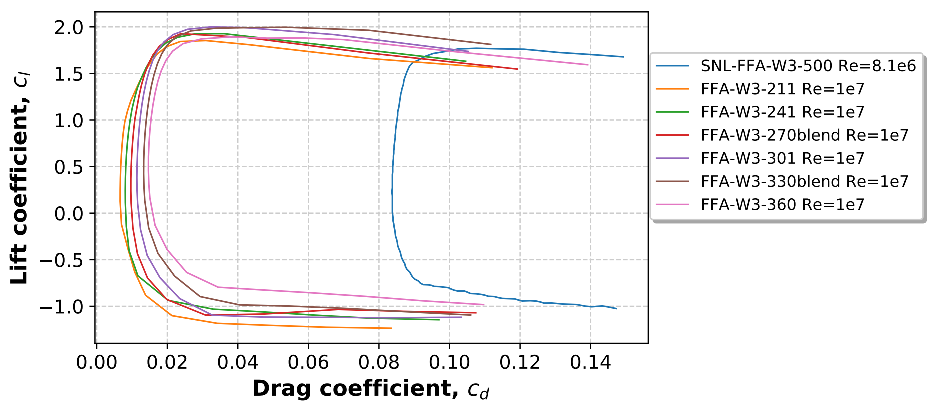

(b) Airfoil lift-drag polars

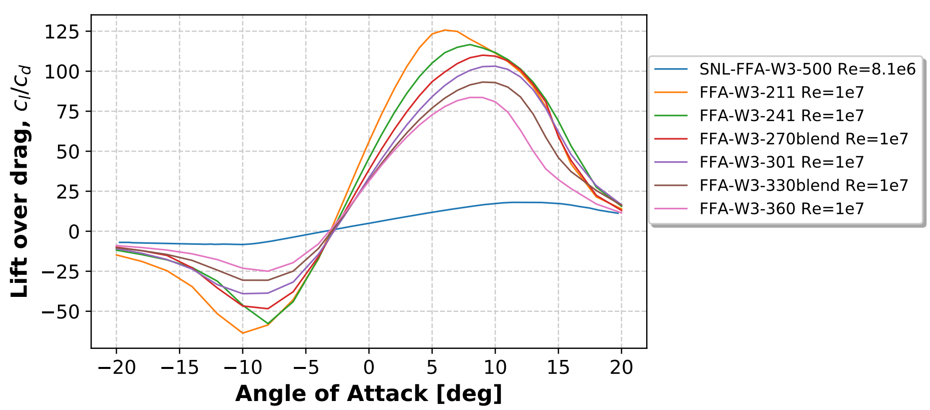

(c) Airfoil lift-to-drag coefficients

Figure 2-3. Aerodynamic polars for the airfoils used on the blade

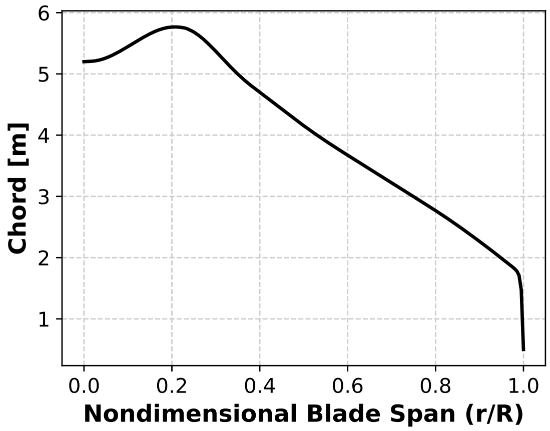

(a) Chord length

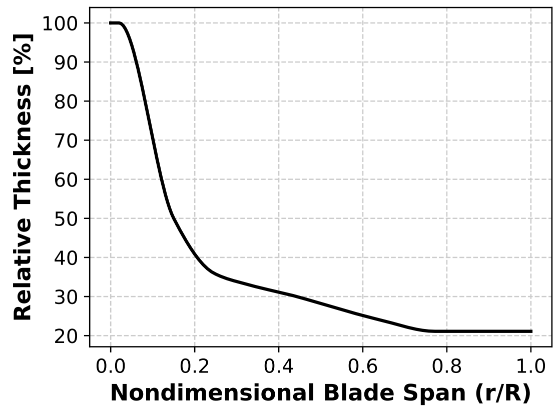

(b) Relative thickness

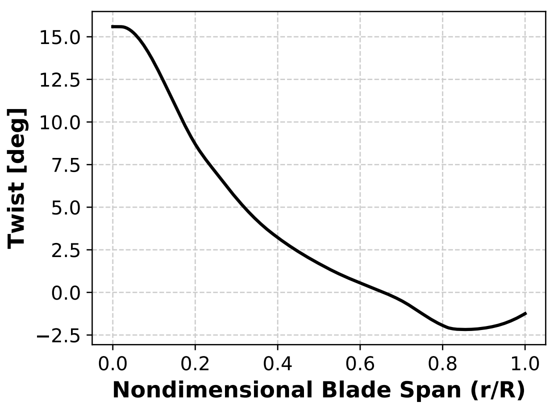

(c) Twist

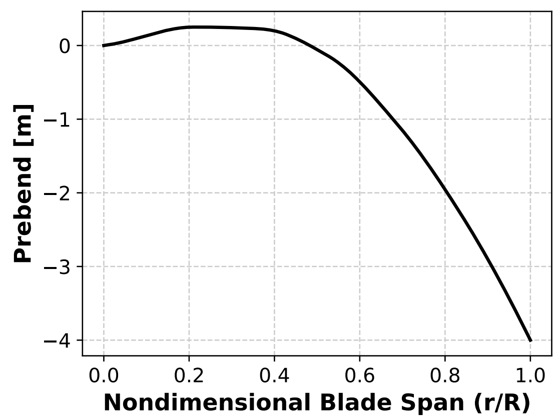

(d) Prebend

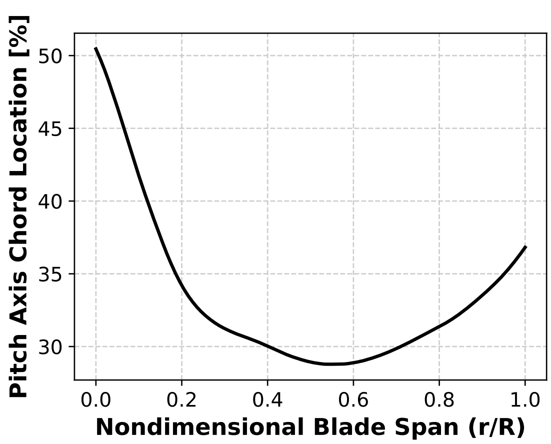

(e) Chordwise offset

Figure 2-4. Blade planform spanwise quantities

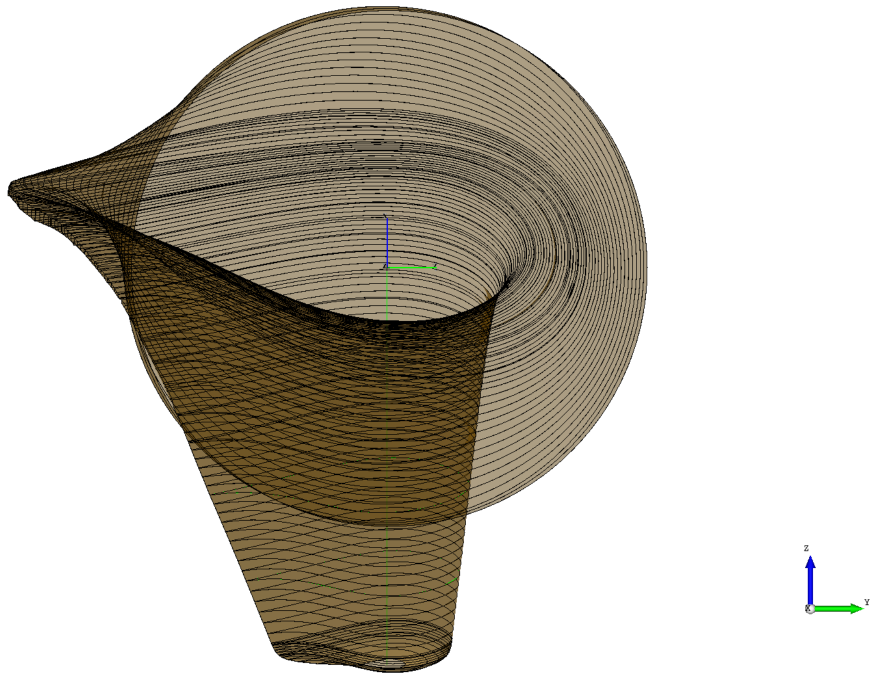

Figure 2-5. Lofted blade shape

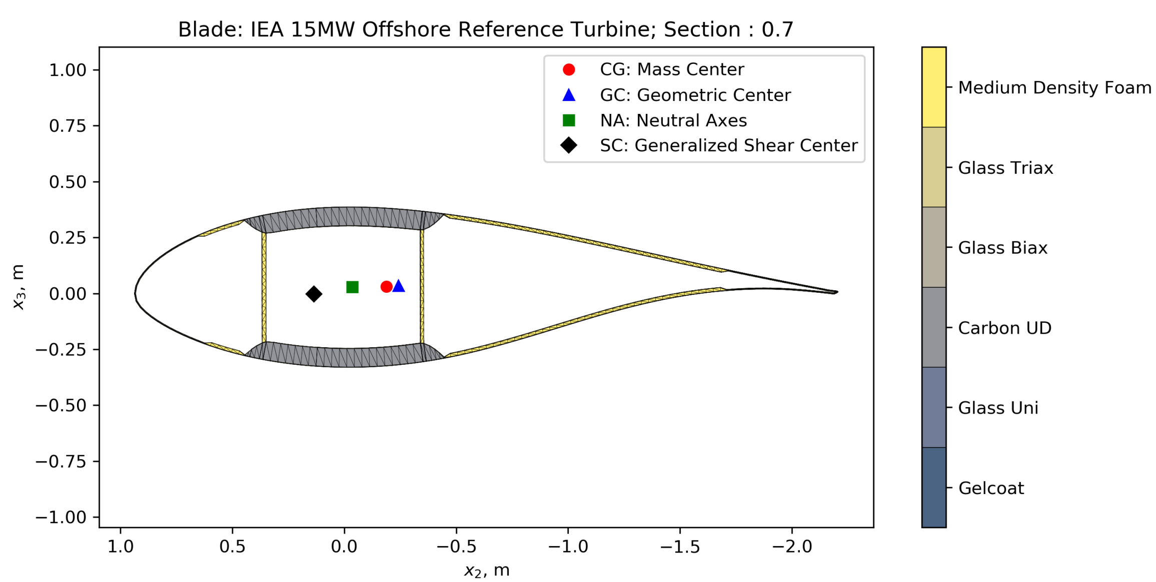

Figure 2-6. Blade cross section at 70% span

The internal structure and composite layup of the blade is defined according to the IEA Wind Turbine Ontology [32]. Composite layers are defined as spanwise elements superimposed on the blade shell or shear webs, following the curved blade reference axis. The wind turbine ontology allows for multiple methods of defining elements, dimensionally, using the layer width (arc length), offset, and rotation relative to a reference position, or nondimensionally, using the normalized arc length positions, as shown in Figure 2-7. The normalized arc length position coordinate (s) is defined as zero at the suction-side trailing edge and as one at the pressure-side trailing edge. For flatback airfoils, the trailing edge is defined as the midpoint of the flatback surface.

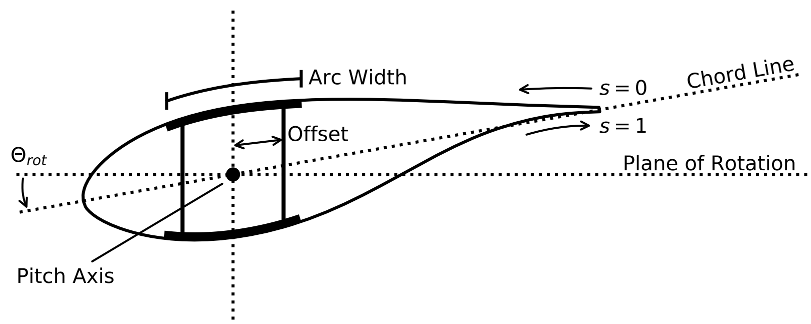

Figure 2-7. Schematic of IEA Wind Turbine Ontology composite definition, from root to tip

The material layup of the blade is plotted in Figures 2-8 and 2-9, shown along the airfoil shell as a function of the arc length s-coordinate and for the shear webs. The complete layup definition of the structural components is provided in the accompanying blade ontology and Microsoft Excel files. With the composite layup defined, the blade beam structural properties were computed with PreComp [16] and VABS [33, 34] (in the NREL tool chain) or BECAS [17, 35] (in the DTU tool chain). Specifically, these tools calculated the stiffness matrices for each cross section along the blade, which were then used in OpenFAST or HAWC2. A comparison of the turbine performance between the NREL and DTU modeling tools is discussed in Rinker et al. [36]. Figures 2-10 and 2-11 show the resulting blade beam structural properties. The structural damping of the first flapwise, edgewise, and torsional modes were assumed to be 3%, 3%, and 6%, respectively.

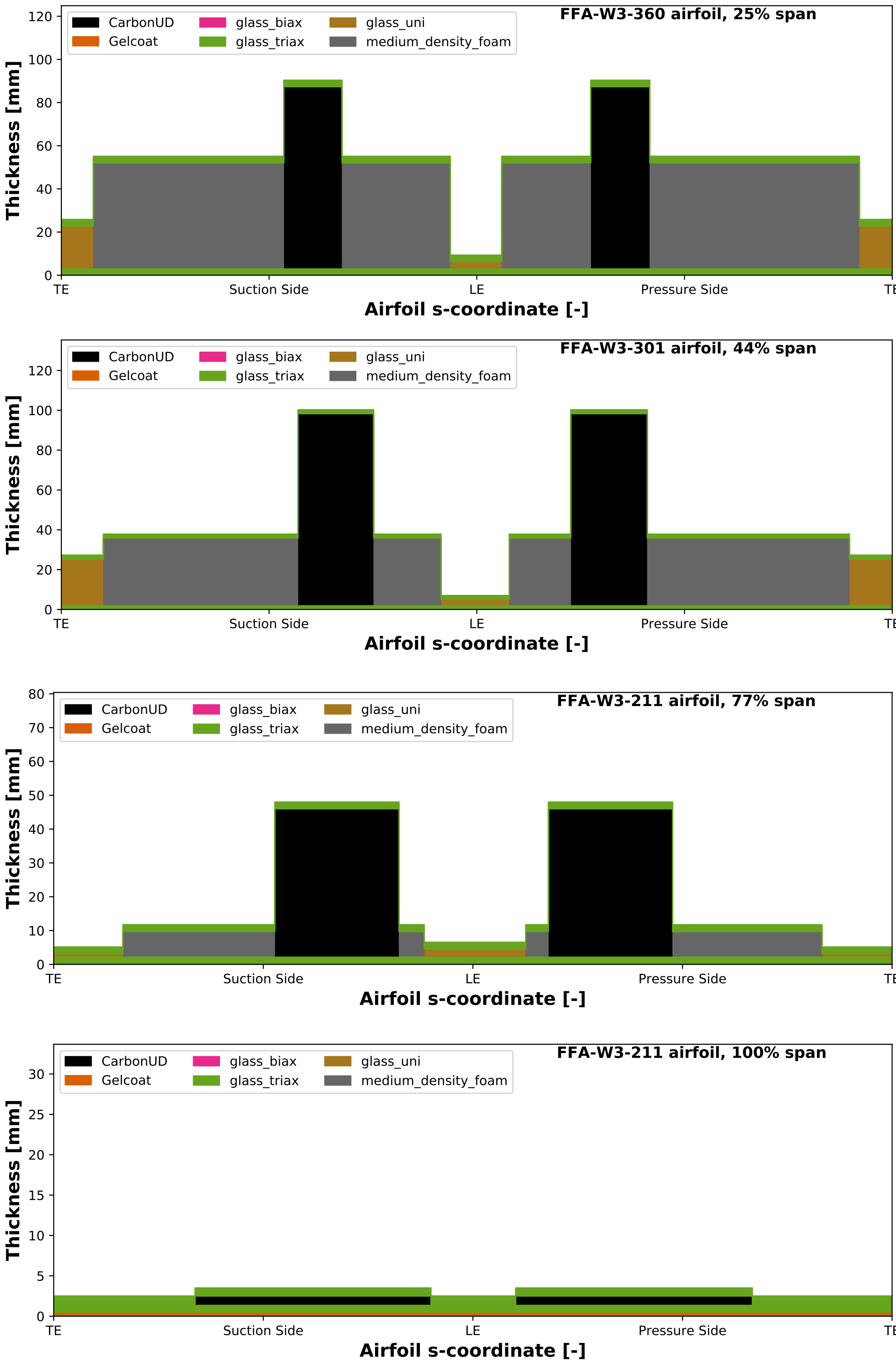

Figure 2-8. Blade layup layer thickness as a function of the normalized s-coordinate around the airfoil at various span positions

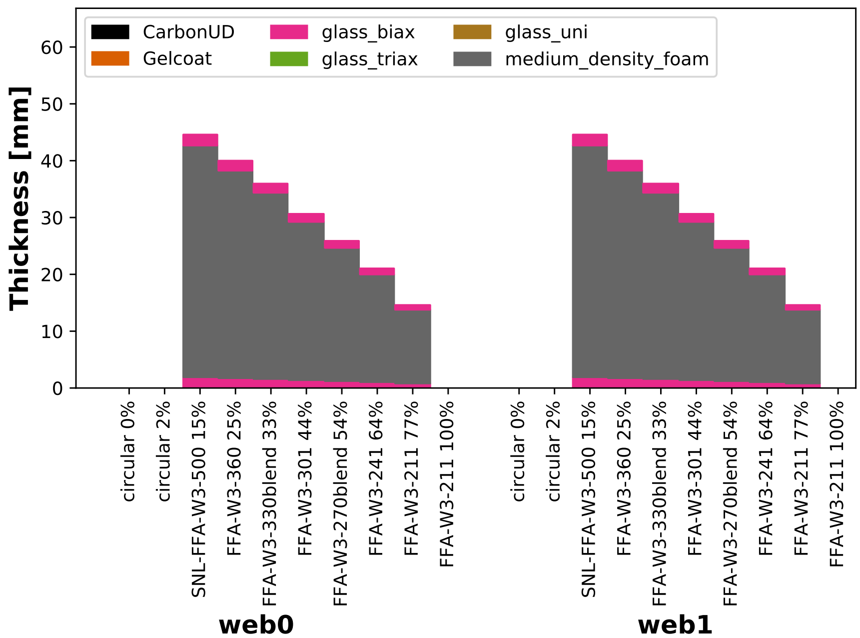

Figure 2-9. Shear layup layer thickness at various span positions

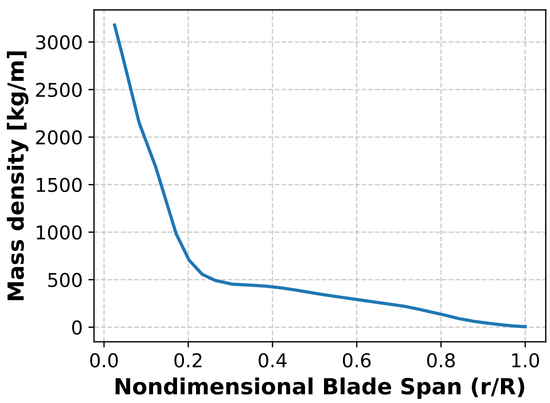

(a) Mass density

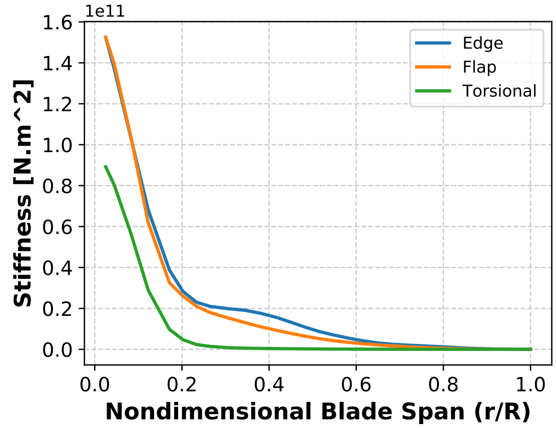

(b) Edgewise, flapwise, and torsional stiffness

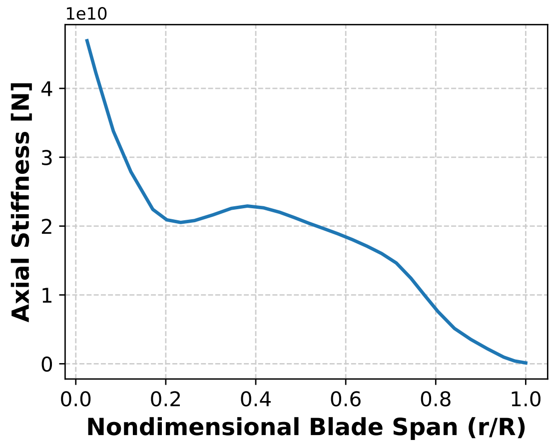

(c) Axial stiffness

Figure 2-10. Blade beam structural properties versus the blade-curve position along the span computed using PreComp

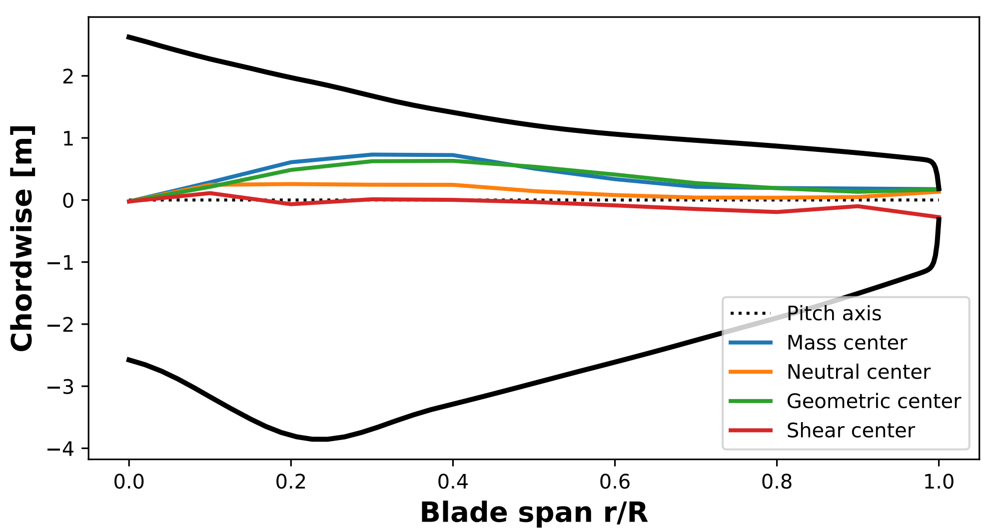

Figure 2-11. Blade planform and structural properties

3 Rotor Performance

Rotor performance is tightly coupled with the controller behavior and pitch schedule to reach the desired shaft revolutions per minute (rpm), torque, and thrust. The controller is described before presenting rotor performance data.

3.1 Controller Properties

Two controllers are provided for the IEA Wind 15-MW reference wind turbine: the NREL Reference OpenSource Controller (ROSCO) [37] and the DTU Basic Controller [38], which are implemented in OpenFAST and HAWC2, respectively. The rotor operates with a minimum rotational speed of 5 rpm to avoid 3-period (3P) interference with the tower/monopile natural frequency, and reaches a rated rotational speed of 7.55 rpm at 10.59 m/s, resulting in a maximum nominal tip speed of 95 m/s. The rotor operates with a pitch setting of 0° at the design tip-speed ratio (TSR), but operates with positive pitch at low wind speeds to track maximum power while maintaining the minimum rotor speed. The rotor starts pitching at the rated wind speed of 10.59 m/s.

3.1.1 Controller Methodology

In both controllers, two active proportional integral (PI) controllers are implemented for the generator torque and blade pitch angles. Saturation limits on rotor speeds and blade pitch angles are implemented to ensure turbine operation within the design constraints. The controller operation can be distinguished by three regions:

3 m/s $\leq U \leq$ 6.98 m/s; minimum rotor speed. A PI controller on the generator torque is used to regulate the turbine to the turbine's minimum rotor speed, 5 rpm. In ROSCO, the minimum blade pitch angle is defined based on a wind speed estimate, such that C_P is maximized. The C_P-maximizing minimum blade pitch angles are found a-priori using steady-state blade element momentum analysis, provided by CCBlade [14]. For the DTU Basic Controller, a PI controller is applied to the torque controller to regulate the rated wind speed. The pitch angles are determined using a look-up table scheduled on the filtered hub-height wind speed.

6.98 m/s $\leq U \leq$ 10.59 m/s; optimal TSR. In below-rated wind speeds, the rotor speed is regulated to operate at the turbine's optimal TSR with a PI controller on the generator torque.

10.59 m/s $\leq U \leq$ 25 m/s; rated power In above-rated wind speeds, the rotor speed is regulated via a PI controller on the blade pitch angle. The objective of the blade pitch controller is to regulate the rotor speed to its rated value, 7.55 rpm. For floating applications, the constant-power setting is traditionally replaced by constant generator torque.

In ROSCO, an extended Kalman-filter-based wind speed estimator is employed to estimate the optimal rotor speeds in below-rated operation and to define minimum blade pitch angles during minimum rotor speed operation. In Region 2.5, instead of the linear constant speed approach used by the NREL 5-MW reference turbine, the ROSCO control uses a setpoint-smoothing methodology [39] to ensure smooth transitions between control regions. As a result of the design optimization process, the IEA Wind 15-MW turbine has a negligible Region 2.5, since the rated rotor speed is reached at rated torque. The PI gains for the generator torque and blade pitch controllers are calculated using the ROSCO generic tuning methodology [39] and included in the accompanying OpenFAST input files.

The parameters for the DTU Basic Controller were determined using HAWCStab2's controller tuning feature. The assumed natural frequencies and damping for the partial-load poles (torque controller) and full-load poles (pitch controller) were 0.05 Hz, 70% critical, and 0.03 Hz, 70% critical, respectively. Quadratic gain scheduling was used with an assumption of constant power. The resulting controller parameters are found in the HAWC2 input files and the definitions for all parameters and Regions 1, 2, and 3 are consistent with the definitions in the DTU Basic Controller report [38].

3.2 Steady-State Performance

Figure 3-1 shows the steady-state performance of the rotor as a function of wind speed, using OpenFAST with the ROSCO controller. In Region 1.5, minimum rotor speed constraints result in significantly higher, suboptimal tip-speed ratios. The blade pitch controller imposes a minimum pitch constraint based on the wind speed estimate, so that C_P is maximized. This results in positive blade pitch angles of up to 4° at low wind speeds. Concurrently, the generator torque controller attempts to set the rotor to the minimum rotor speed in Region 1.5. In Region 2, the torque controller tracks the set point tip-speed ratio, which is set near or at maximum C_P. The design point for this blade is TSR =9.0 and blade pitch Θ_{pitch} =0°, which is slightly below the optimal of TSR =8.5 and Θ_{pitch} =−1.0°, shown in the C_P and C_T curves in Figure 3-2. This slightly suboptimal design point is a result of the blade design process, as a trade-off between power production and design constraining loads. The set point smoothing routine in ROSCO prevents contradictions between the generator torque and blade pitch controllers during Region 2.5 transitions. The Region 2.5 for this design is effectively negligible, so there is little influence from the set point smoothing and peak shaving routines in ROSCO. Finally, in Region 3, the torque controller is saturated at rated torque and the blade pitch PI controller pitches to feather to maintain rated rotor speed.

Further analysis of the blade performance is shown in Figure 3-3. Here, the distributed aerodynamic forces on the blade are computed over a range of below-rated wind speeds. In Section 2, the aerodynamic design of the blade, especially the twist, was presented as tightly constrained by the tip deflection and tower clearance constraints. Forces on the blade peak at approximately 90 m and then begin to decrease toward the tip. This unloading of the blade tip helps prevent tower strikes; however, it results in lost power production, especially because the blade tip has the highest aerodynamic efficiency and marginal swept area. The sharp, linear drop for the outboard 5% of the blade is caused by the Prandtl tip loss model employed in the aeroelastic simulations.

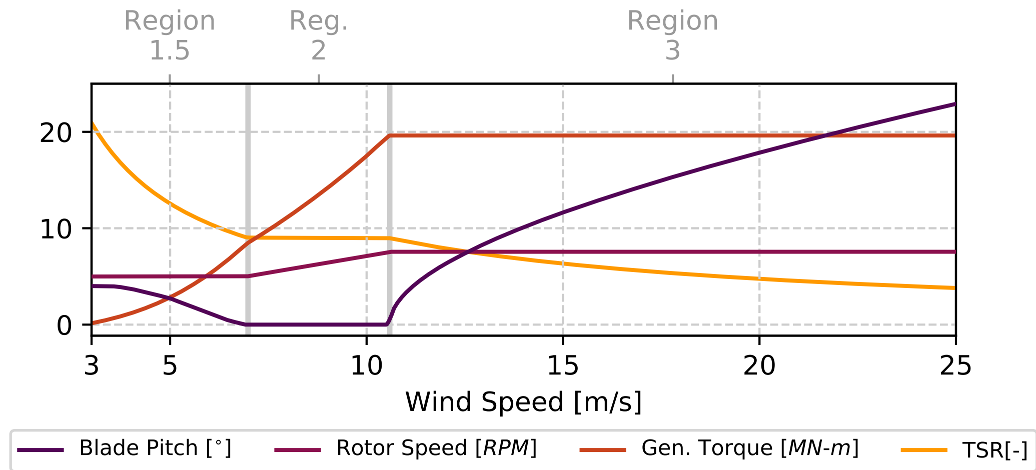

(a) Controller regulation trajectory

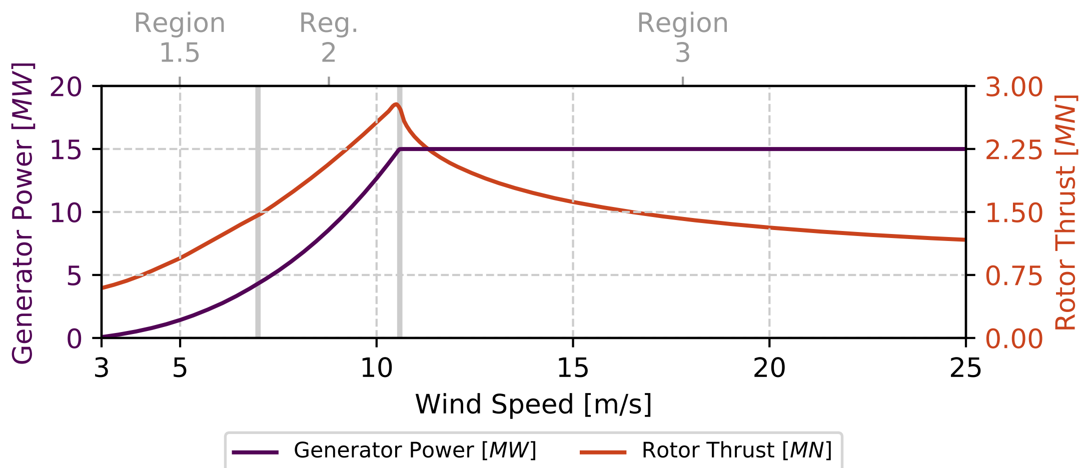

(b) Power and thrust curve

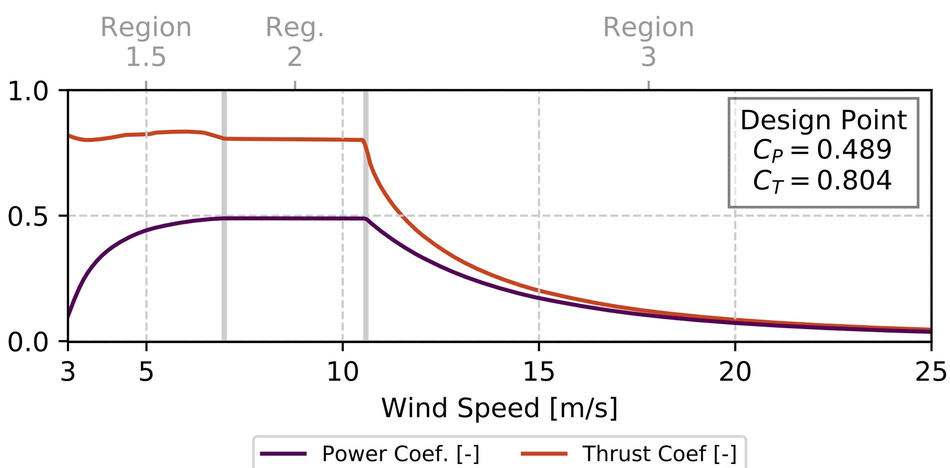

(c) Aerodynamic performance coefficients

Figure 3-1. OpenFAST blade element momentum performance and operation of the 15-MW rotor with the ROSCO controller

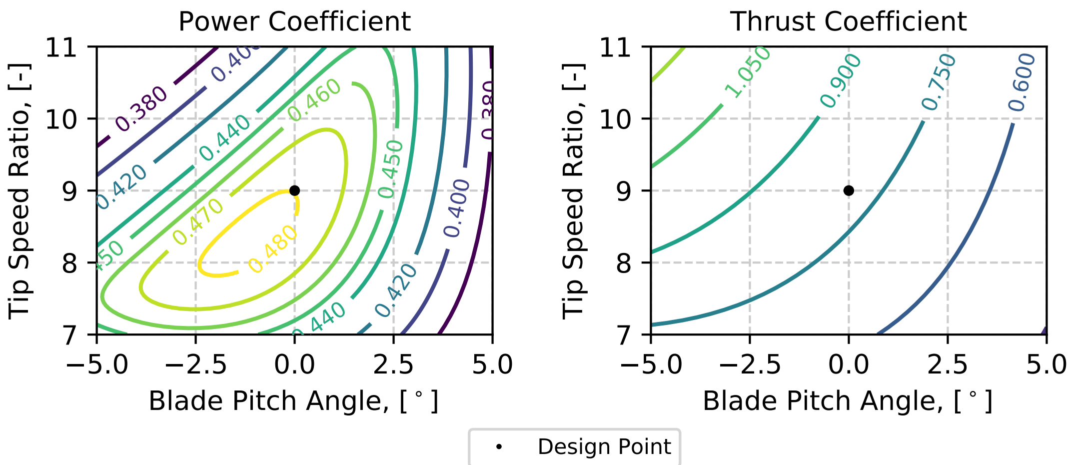

Figure 3-2. CCBlade steady-state blade element momentum aerodynamic power and thrust coefficient surfaces as a function of blade pitch and TSR

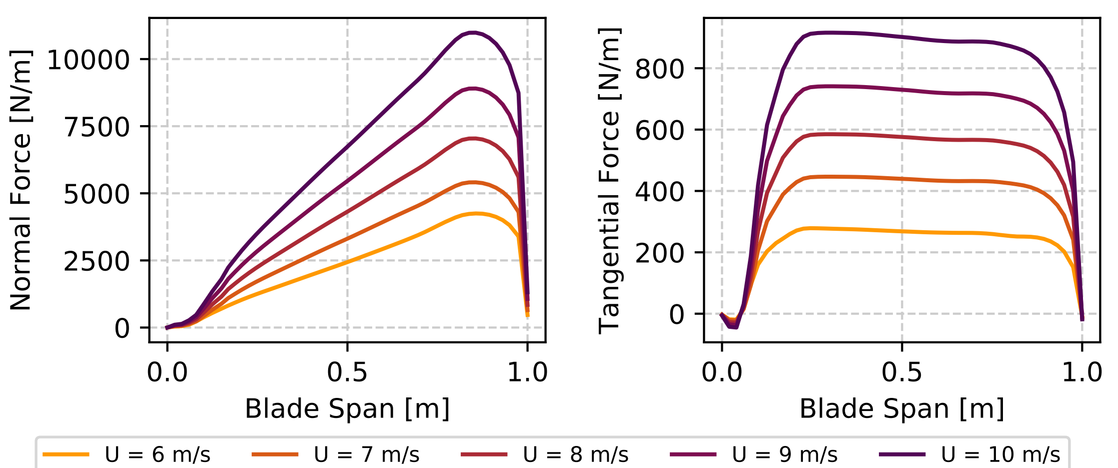

Figure 3-3. Spanwise forces on the blade as a function of wind speed

4 Tower and Monopile Properties

The tower and monopile were designed as an isotropic steel tube in WISDEM and OpenFAST. The monopile design was informed by the helpful guide published by Arany [40]. Frequency considerations constrained much of the design in that the first tower-monopile mode, 0.170 Hz, lies between the 1P and 3P blade passing frequency ranges for all wind speeds, as shown in Figure 4-1. This is also sufficient to avoid the range of expected ocean wave frequencies for the generic East Coast site: 0.10 Hz to 0.13 Hz. Note that when a floating substructure is used, the frequency requirements and boundary conditions will shift such that a stiffer tower is required. Therefore, the tower geometry presented here will be replaced with one better suited for a semisubmersible platform.

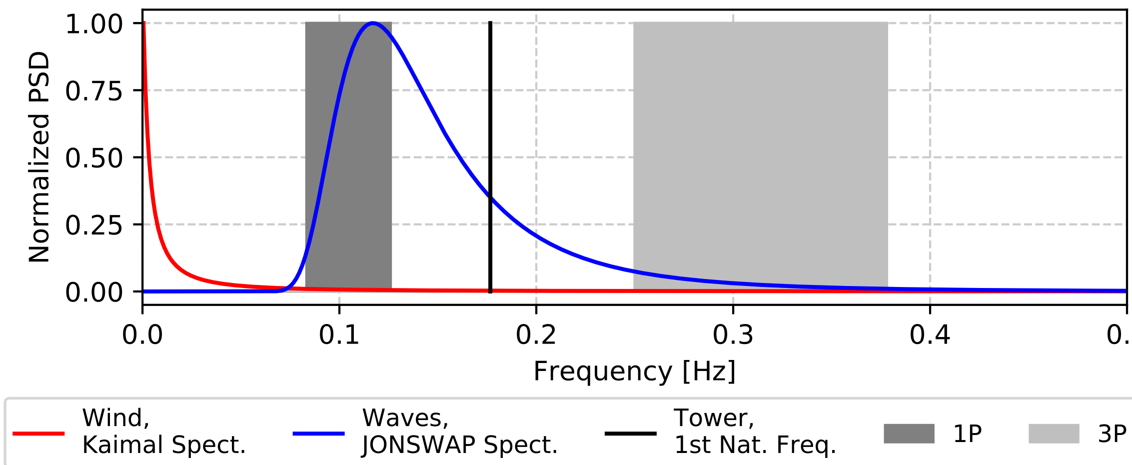

Figure 4-1. Tower natural frequency relative to the normalized power spectral density (PSD) of the excitation frequencies

The tower height was chosen such that the hub height reaches 150 m, allowing for 30 m of ground (water surface) clearance with 120-m blades.[1] The monopile foundation has a 10-m outer diameter, which pushes the limits of current manufacturing and installation technology. The thickness and outer diameter are shown in Figure 4-2 and tabulated in Table 4-2, down through the embedded suction pile. The material properties are stated in Table 4-1.

A detailed geotechnical analysis of soil properties was not conducted as part of this design effort. Instead, the soil foundation was modeled with a series of spring constants to represent the soil stiffness in a one-dimensional finite-element model. The selected summary values for soil shear modules and Poisson's ratio are representative of dense sand or gravel soils [41]. The equations for the soil stiffness sprint constants are found in Appendix B.2.

Table 4-1. Material Properties for the Tower

Parameter	Symbol	Value	Units
Young's modulus, steel	E	2 00E11	Pa
Shear modulus, steel	G	7 93E10	Pa
Density, steel	ρ	7 85E3	kg/m^3
Shear modulus, soil	G_s	140E6	Pa
Poisson's ratio, soil	ν_s	0.4	

Pa pascal kg/m^3 kilogram per cubic meter

Both HAWC2 and OpenFAST require a number of structural cross-sectional properties that can be easily determined from the diameter and wall thickness profiles. These properties are shown in Figure 4-3, with the underlying equations provided in Appendix B. Note that the final mass values reported in Table 1-1 include an extra 7% of outfitting mass beyond the cylindrical shell mass and 100 t for the transition piece.

[1] The 30-m clearance value is not specified in an official standard and offshore wind turbine clearances can vary between 20 m to 30 m.

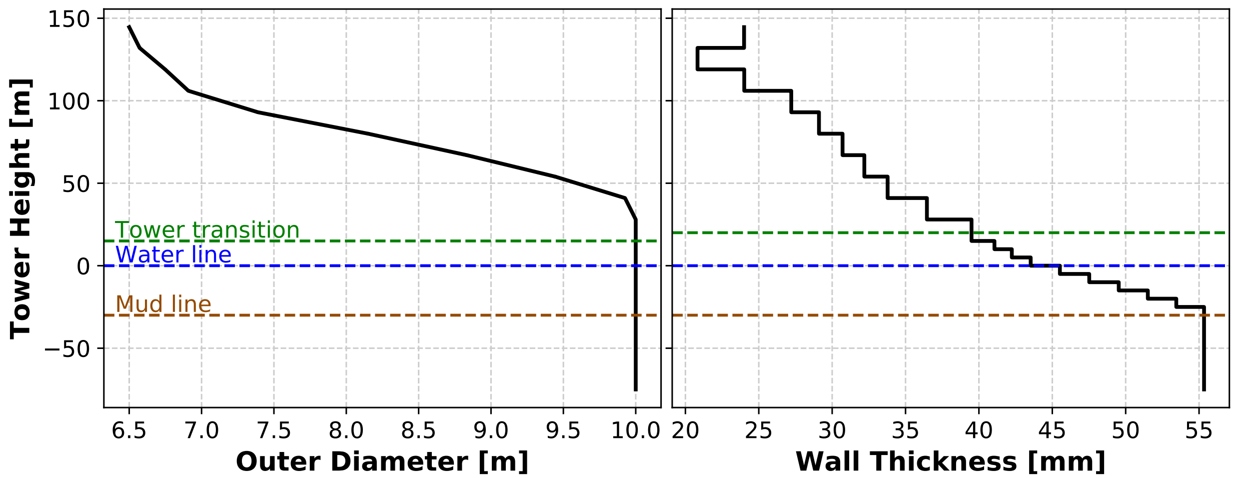

Figure 4-2. Outer diameter and wall thickness for tower

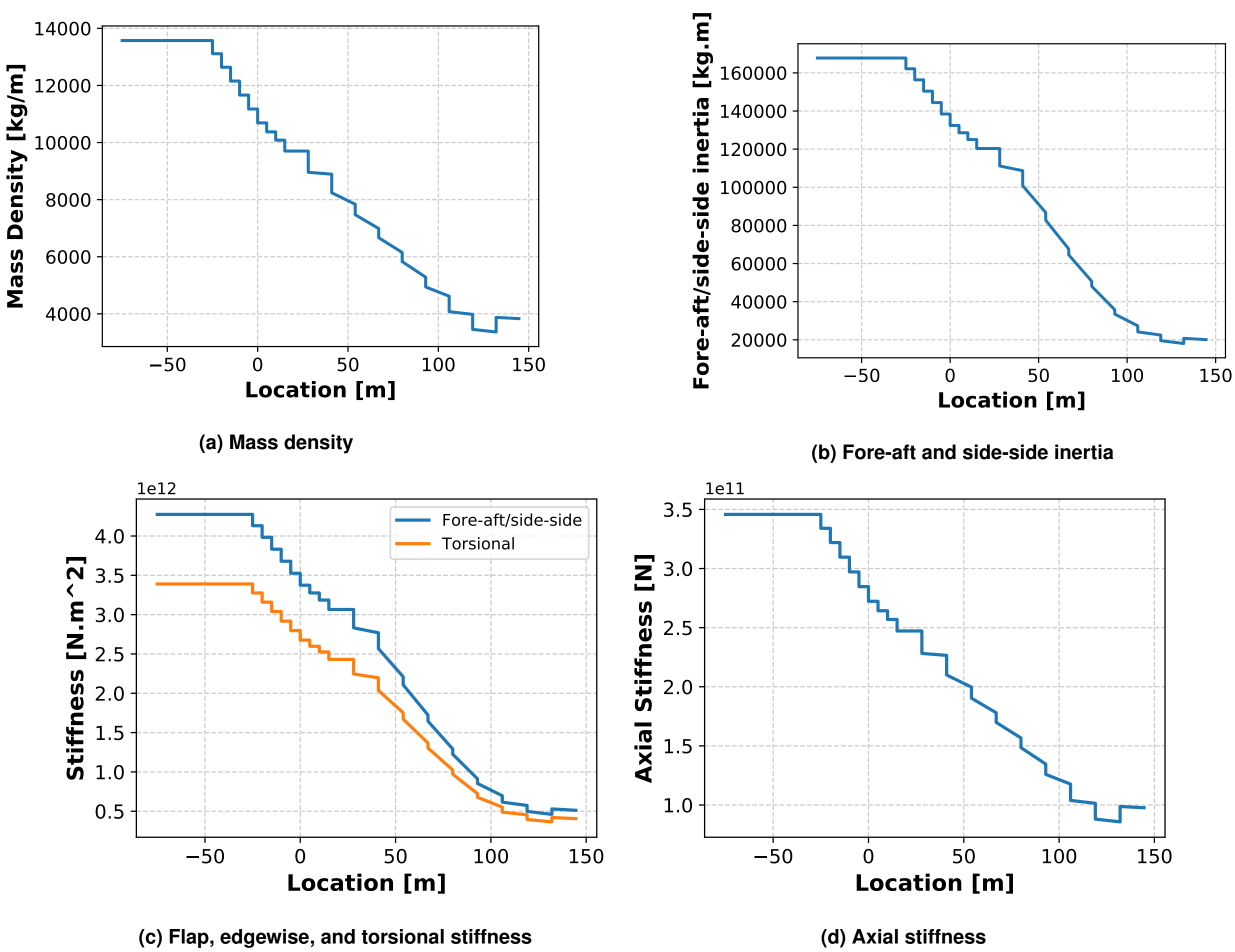

Figure 4-3. Tower and monopile cross-sectional properties

Table 4-2. Some Key Properties and Dimensions of the Tower and Foundation

Location	Height [m]	Outer Diameter [m]	Thickness [mm]
Monopile start	-75.000	10.000	55.341
Mud line	-30.000	10.000	55.341
	-29.999	10.000	55.341
	-25.000	10.000	55.341
	-24.999	10.000	53.449
	-20.000	10.000	53.449
	-19.999	10.000	51.509
	-15.000	10.000	51.509
	-14.999	10.000	49.527
	-10.000	10.000	49.527
	-9.999	10.000	47.517
	-5.000	10.000	47.517
	-4.999	10.000	45.517
Water line	0.000	10.000	45.517
	0.001	10.000	43.527
	5.000	10.000	43.527
	5.001	10.000	42.242
	10.000	10.000	42.242
	10.001	10.000	41.058
Tower start	15.000	10.000	41.058
	15.001	10.000	39.496
	28.000	10.000	39.496
	28.001	10.000	36.456
	41.000	9.926	36.456
	41.001	9.926	33.779
	54.000	9.443	33.779
	54.001	9.443	32.192
	67.000	8.833	32.192
	67.001	8.833	30.708
	80.000	8.151	30.708
	80.001	8.151	29.101
	93.000	7.390	29.101
	93.001	7.390	27.213
	106.000	6.909	27.213
	106.001	6.909	24.009
	119.000	6.748	24.009
	119.001	6.748	20.826
	132.000	6.572	20.826
	132.001	6.572	23.998
Tower top	144.582	6.500	23.998

The damping for the tower is stiffness-proportional only. For both OpenFAST and HAWC2, the stiffness-proportional factors were determined by enforcing a 2% logarithmic decrement on the first fore-aft, side-side, and torsional tower modes (modes 1, 2, and 7, respectively). The final model-specific values can be found in the respective input files.

5 Nacelle, Drivetrain, and Hub

The IEA Wind 15-MW reference wind turbine uses a direct-drive layout with a permanent-magnet, synchronous, radial flux generator in a simple and compact nacelle layout. Direct-drive wind turbine generators offer a number of advantages over geared drivetrains, including fewer parts, lower complexity, higher reliability, and additional flexibility in designing for special topologies. However, the direct coupling of the generator at very low speeds requires large physical dimensions and higher mass, which incur transportation, assembly, and servicing challenges. Countering these challenges involves an optimal balance of generator location, the number of bearings, internal or external stator/rotor arrangement, rotor/stator inactive substructure geometries, ancillary component interfaces, among other considerations [42].

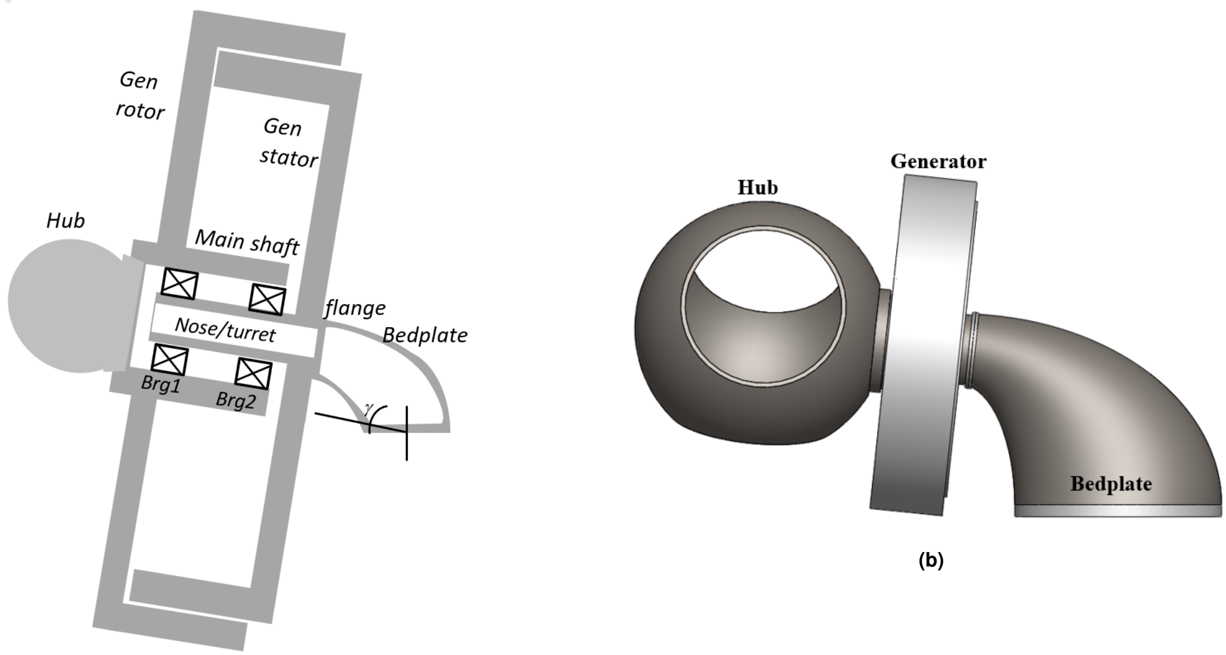

(b)

(a)

Figure 5-1. A sketch and CAD model of the nacelle layout of the 15-MW direct-drive wind turbine. Not to scale and some structural details omitted. Blades (not shown), hub, shaft, and generator rotor rotate.

5.1 Nacelle Overview

Figure 5-1a shows a simple direct-drive nacelle layout with an outer-rotor permanent-magnet generator. The assembly consists of a hub shaft supporting the turbine and generator rotors on two main bearings housed on a stationary turret that is cantilevered from the bedplate. The bedplate transmits the hub loads and weight of the rotor, generator, hub, shaft, and turret to the tower. The three-dimensional CAD illustration is shown in Figure 5-1b. In determining the optimal dimensions of the various components, the highest acceptable equivalent von Mises stress under extreme aerodynamic loads measured during extreme turbulence conditions was 200 mega pascal (MPa). These ultimate loads were assumed to represent multiaxial loading under these conditions, as suggested by International Electrotechnical Commission (IEC) 61400-1. The full mass breakdown of the nacelle and its components is summarized in Table 5-1.

5.2 Hub

The hub design is based on a simple spherical hub shell model with cutouts for the blades and the flange. The hub diameter is calculated as a function of the blade root diameter. The thickness of the hub shell is designed to with-

Table 5-1. Lumped Masses and Moments of Inertia for the Nacelle Assembly

(The coordinate system has its origin at the tower top, with x pointed downwind [parallel to ground/water and not the shaft] and z pointed up)

Name	X_{TT} [m]	Z_{TT} [m]	Mass [t]	I_{xx} [kg m^2]	I_{yy} [kg m^2]	I_{zz} [kg m^2]
Yaw system	0.000	-0.190	100.0	490,266	490,266	978,125
Turret nose	5.786	4.956	11.394	12,571	10,890	10,909
Inner generator stator	5.545	4.913	226.629	3,777,313	2,012,788	2,042,312
Outer generator rotor	6.544	5.033	144.963	3,173,003	1,673,269	1,691,864
Shaft	6.208	5.000	15.734	33,009	22,906	23,018
Hub	10.604	5.462	190.0	1,382,171	2,169,261	2,160,637
Bedplate	0.812	2.697	70.329	398,973	515,880	535,055
Flange	4.593	4.831	3.946	4,081	2,065	2087
Misc. equipment	0.000	0.500	50.0	16,667	16,667	25,000
TDO shaft bearing	6.582	5.040	2.230	3,515	1,784	1,803
SRB shaft bearing	5.388	4.914	5.664	8,930	4,593	4,641
Nacelle total	5.486	3.978	820.888	12,607,277	21,433,958	18,682,468
Nacelle total minus hub	3.945	3.352	630.888	10,680,747	122,447,810	10,046,187

kg m^2	kilogram square meters	m	meters	t	metric tons
TDO	tapered double outer	SRB	spherical roller bearing		

stand the forces generated in an emergency shutdown event. The hub flange diameter is half of the hub diameter, and the flange thickness is four times the thickness of the hub shell. Edges of the flange are designed to minimize stress concentrations. The pitch system is not modeled in extensive detail and its mass is estimated using regression fits.

5.3 Main Shaft, Bearings, and Turret

A depiction of the main shaft, bearings, and turret is shown in Figure 5-2, with key parameters and dimensions listed in Table 5-2. The main shaft has a hollow cylindrical cross section, with a constant wall thickness and a tilt angle of 6°. The main shaft, along with the rotor, is supported by two main bearings. Both these main bearings have rotating outer raceways and fixed inner raceways. The outer raceways and bearing housing are accommodated by a turret held by the bedplate. The entire weight of the turbine rotor, generator rotor, and hub loads are transmitted by the main shaft to the turret via the bearings.

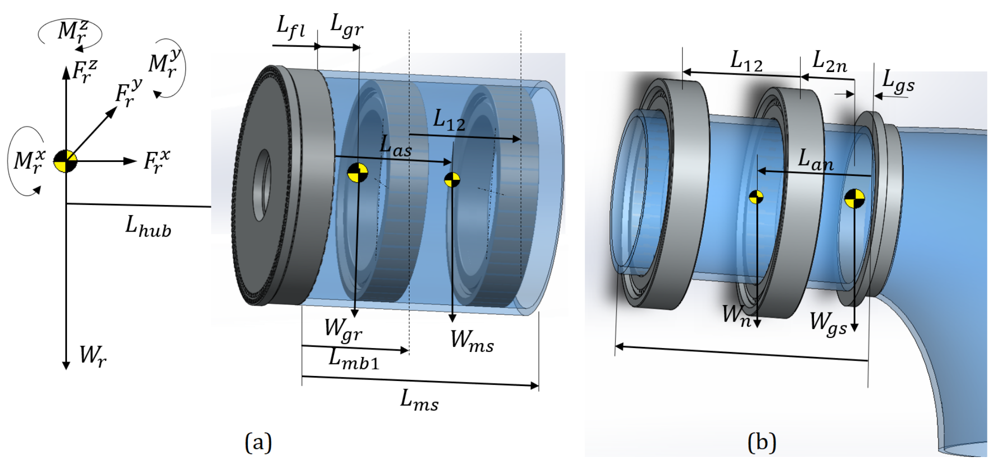

Figure 5-2. CAD illustration of (a) the main shaft and (b) turret (also called the nose); dimensions are documented in Table 5-2

The inner diameter of the main shaft was designed with sufficient clearance for the nacelle turret and the main bearings. The thickness of the shaft was determined by ensuring a safe load path from the rotor while limiting the maximum deflection at the generator. It is assumed that the entire thrust load is transmitted by the main shaft to the upwind main bearing.

The turret also has a hollow cylindrical cross section, with a constant wall thickness cantilevered from the bedplate. The inner diameter was set to 2 m to provide clearance for technician access. The thickness of the turret cylinder was determined by computing the reactions from the main bearings while limiting the maximum radial deflections at the interface with the generator rotor and stator. It is assumed that the turret carries all of the thrust imparted by the upwind main bearing, the moments from the transverse forces, and the torque.

The paired set of bearings consists of a fixed upwind bearing and floating downwind bearing. A tapered double outer configuration was chosen for the locating bearing and a spherical roller bearing for the nonlocating bearing. The chosen bearing solutions were based on recommendations found in [43], with a basic lifetime estimation for ultimate loads, as described in the DNV guidelines. Loads from the aeroelastic simulations were used to determine the reactions at the main bearings. The upwind bearing was assumed to carry all axial loads and moments, whereas both the upwind and downwind bearings share the radial forces. These forces were directly transmitted to the turret and from there to the bedplate and tower. Because the downwind bearing carries smaller loads, we propose a bearing with a lower load rating.

Table 5-2. Main Shaft Dimensions, Bearing, and Loads Used in Sizing

Symbol	Description	Value	Units
L_{fl}	Hub flange length	0.358	m
L_{mb1}	Distance of upwind bearing	1.0	m
L_{gr}	Generator rotor location	0.1	m
L_{12}	Distance between upwind and downwind bearings	1.2	m
L_{as}	Main shaft center of mass	1.25	m
γ	Shaft tilt angle	6.0	deg
L_{ms}	Length of main shaft	2.2	m
R_{osh}	Outer radius of the main shaft	3.0	m
R_{ish}	Inner radius of the main shaft	2.8	m
L_{gs}	Location of generator stator from bedplate flange	0.25	m
L_{an}	Turret center of mass	1.2	m
L_{2n}	Distance of downwind bearing from bedplate flange	0.9	m
L_{an}	Turret length	2.2	m
R_{on}	Outer radius of the turret	2.2	m
R_{in}	Inner radius of the turret	2.0	m
$Mb1$	Tapered double outer ring: mass	2,230	kg
$Mb2$	Spherical roller bearing: mass	5,664	kg

deg degrees m meters kg kilograms

5.4 Bedplate

The bedplate is a hollow, elliptically curved, cantilever beam with circular cross sections. The bedplate has a smaller cross section that interfaces with the bedplate flange and a larger cross section that interfaces with the yaw bearing at the tower top. The thickness of the circular ring elements is optimized to constrain the cumulative stresses from bending, torsion, shear forces, and axial loads to 200 MPa. The total end deflection is an input into the turret design for an accurate air-gap deflection estimate. The driving load case is taken from the extreme aerodynamic and turbulent wind field. Figure 5-3 shows the CAD illustration of the bedplate design based on the critical dimensions provided in Table 5-3.

5.5 Yaw System

The yaw system bearings are based on those available in SKF's catalog, specifically double-row, angular, contact ball bearings. The yaw system mates the bedplate base with the tower top at a diameter of 6.5 m.

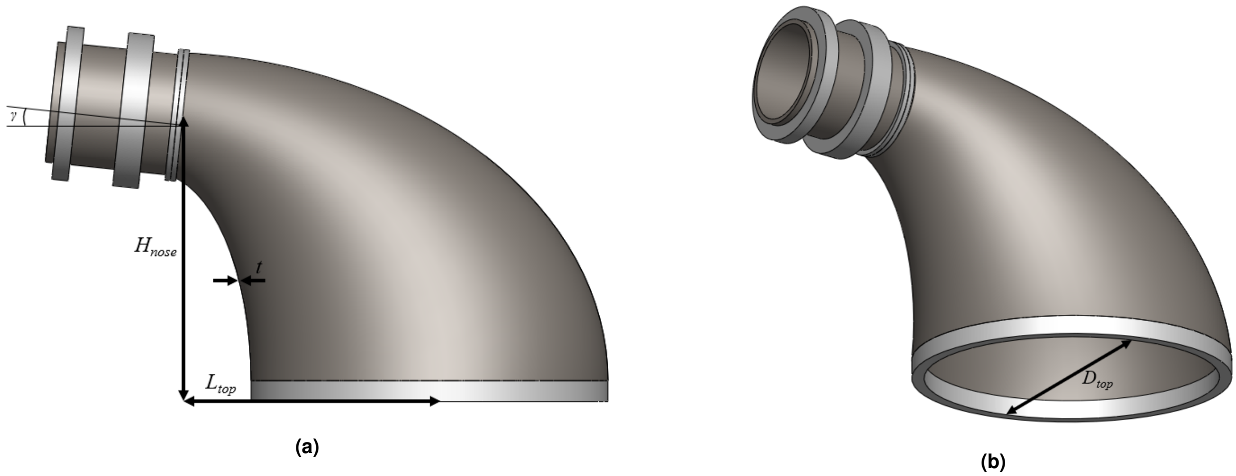

Figure 5-3. A CAD illustration of the bedplate

.

Table 5-3. Bedplate Properties

Symbol	Description	Value	Units
L_{top}	Tower top distance from turret flange	5	m
H_{nose}	Nose height	4.875	m
D_{top}	Tower top diameter	6.5	m
t	Bedplate wall thickness	50	mm
$M_{bedplate}$	Bedplate mass	70,329	kg

kg kilograms m meters mm millimeters

5.6 Direct-Drive Generator

The DrivetrainSE module within WISDEM [44] was used to design and optimize a 15-MW direct-drive synchronous generator. The generator construction features an external rotor radial flux topology machine with a surface-mounted permanent magnet (shown in Figure 5-4), with the design and performance parameters listed in Table 5-4. The outer rotor layout facilitates a simple and rugged structure, easy manufacturing, short end windings, and better heat transfer between windings and teeth than the inner rotor configuration. The stator design features fractional slot layout double-layer concentrated coils, which maximize the fundamental winding factor. The design optimization followed the guidance found in [45–47]. The guiding assumptions in the design include the following:

- The rotor magnets comprise N40-grade sintered neodymium (NdFeB) magnets, with a remnant flux density of 1.28 tesla (T) and relative permeability of 1.06.
- Only radial components of the air-gap flux are considered, meaning leakage and fringing effects are neglected.
- A slot-pole combination of 2–5 was chosen to derive the concentrated winding layout using Cro's technique and winding vector method [45].
- The magnet width was assumed to be 80% of the pole pitch.
- The design is symmetric and the magnetic circuit is not saturated.
- The magnetic and electrical loadability are determined for a typical tangential stress of 60 kPa. The specific current loading is assumed to be less than 100 kilo-ampere (kA) per meter, provided that an efficient thermal management system is in place so that the output power of the machine can be improved without increasing its size.
- Single-sided disc-type support structures are assumed to hold the electromagnetically active materials to greatly simplify the assembly.
- The air-gap length is assumed to be 1/1,000th of the air-gap diameter. The air gap is allowed to deflect by up to 20%, with the support structure, shaft, and turret contributing to the deformation.

The optimized design features 100 pole pairs dispersed in an air-gap diameter of 10.53 m, a stack length of 2.17 m, and an efficiency of 96.5%. The generator weighs 372 t, split between 227 t for the stator and 145 t for the rotor. At least 50% of the mass stems from the structural support.

5.7 Nacelle Damping

We chose the stiffness-proportional damping for the shaft to produce 5% of critical modal damping for the free-free mode of the generator/rigid-rotor system. This value was chosen based on the value in the NREL 5-MW reference model. In particular, it can be shown that the stiffness proportional term, β, should be chosen such that:

$$\beta = 2\zeta\sqrt{\frac{I_{gen}I_{rot}}{K_{DT}(I_{gen}+I_{rot})}}, \tag{5.1}$$

where ζ is the desired modal damping, I_i is the generator or rotor inertia, and K_{DT} is the equivalent stiffness of the drivetrain. For this turbine, the rigid rotor inertia is approximately $3.524\,605 \times 10^8$ kilogram-square meters (kgm^2), calculated from the HAWC2 blade structural file while ignoring coning and prebend. This results in $\beta = 4.457\,544 \times 10^{-4}$ for the torsional motion.

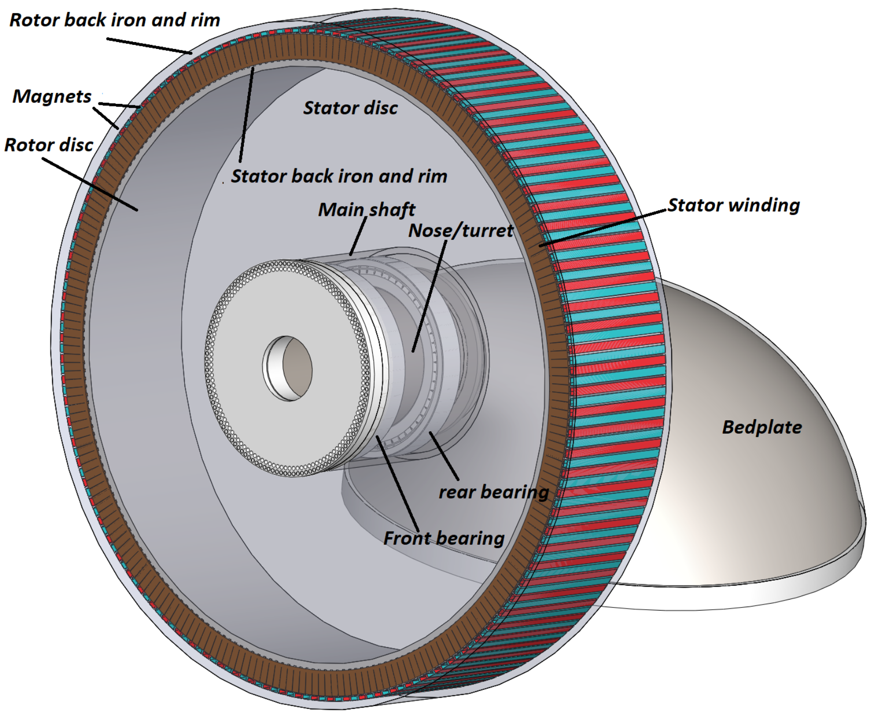

(a) CAD layout

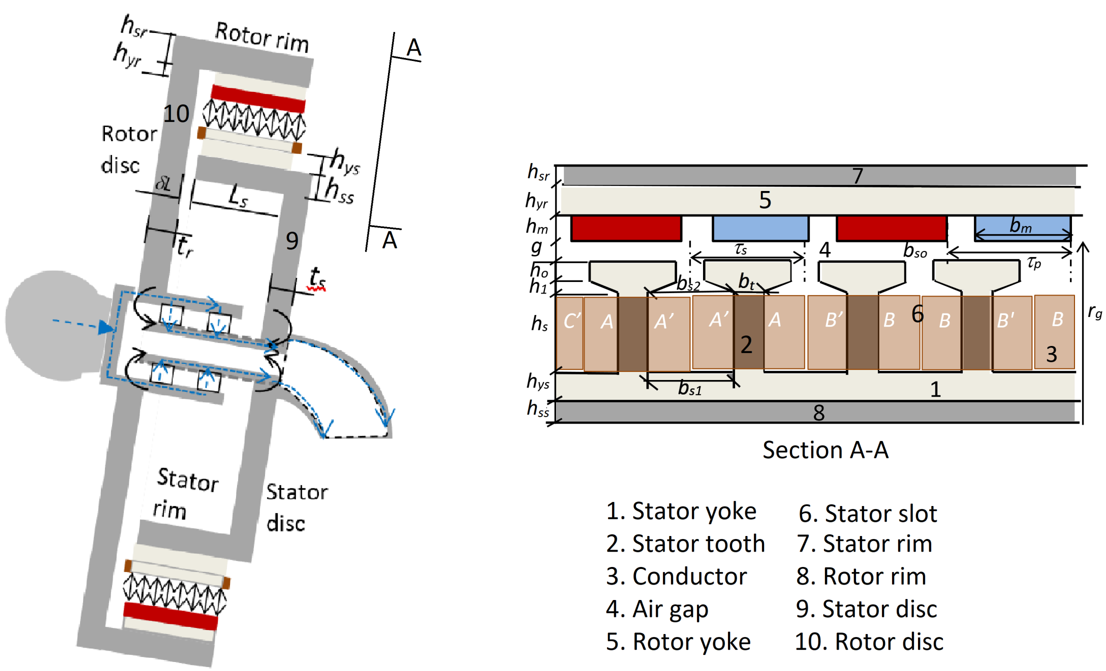

(b) Design parameters

Figure 5-4. A CAD illustration of an outer rotor direct-drive generator with electromagnetic and structural design parameters

Table 5-4. Electromagnetic and Structural Design of the 15-MW Direct-Drive Generator

Symbol	Description	Value	Units
P_r	Rated power at generator terminals	15	MW
ω_r	Rated speed	0.792	rad/s
f_e	Electrical frequency	12.6	Hz
T_r	Rated torque	21.03	MN m
	Electromagnetic Design		
r_g	Air-gap radius	5.08	m
l	Core length	2.17	m
g	Air-gap length	10.16	mm
p	Poles	200	-
S	Stator slots	240	-
h_{ys}	Stator yoke thickness	46.52	mm
h_{yr}	Rotor yoke thickness	63.62	mm
τ_p	Pole pitch	159.55	mm
τ_s	Slot pitch	132.7	mm
h_s	Slot height	400.03	mm
b_s	Slot width	57.3	mm
b_t	Tooth width	74.85	mm
h_m	Magnet height	58.39	mm
b_m	Magnet width	127.64	mm
V	RMS line voltage	4770.34	V
I	Nominal winding current (RMS)	1084.55	A
R_s	Stator winding resistance per phase	0.16	Ω
N_s	Stator winding turns per phase	320	-
$\hat{B}_g$	Peak air-gap flux density	1.06	T
J_s	Winding current density	3.39	A/mm^2
A_1	Specific current loading	92.46	kA/m
η	Efficiency at full load	96.55	%
M_{Iron}	Iron mass	180.95	t
M_{Cu}	Copper mass	9.01	t
M_{Magnet}	Magnet mass	24.20	t
M_{Active}	Total active mass	214.16	t
	Structural Design		
h_{ss}	Stator rim thickness	46.59	mm
t_s	Stator disc thickness	79.97	mm
h_{sr}	Rotor rim thickness	63.69	mm
t_r	Rotor disc thickness	81.75	mm
δ_l	Rotor stator clearance	825	mm
M_{SStru}	Total rotor structural steel mass	86.2	t
M_{RStru}	Total stator structural steel mass	71.1	t
M_{Gen}	Estimated total generator mass	371.57	t

MW	megawatts	V	volts
rad/s	radians per second	A	amperes
Hz	hertz (cycles per second)	Ω	ohms
MN m	mega-newton meters	T	tesla
m	meters	A/mm^2	amperes per square millimeter
mm	millimeters	kA/m	kilo-amperes per meter
t	metric tons		

6 Load Assessment

An IEC design load case (DLC) [4] analysis study was conducted to determine the worst-case ultimate loading on key design constraining components. Table 6-1 provides details on the DLC cases simulated in OpenFAST and Table 6-2 specifies the corresponding metocean inputs. The maximum bending moments and deflections across all cases were ranked, as shown in Figure 6-1 and Figure 6-2. Yaw-misaligned parked conditions with extreme wind speeds and extreme coherent gust with a direction change result in the worst-case loading for this design. The worst-case out-of-plane tip deflection is 22.8 m, leaving more than sufficient tower clearance, with an unbent blade tip-to-tower clearance of 30.0 m. This margin suggests that the blade design is conservative and further aeroelastic optimization could potentially improve the aerodynamic performance or cost of energy while still remaining within recommended safety margins. A full fatigue analysis of this blade was not conducted, which could potentially be an issue for the edgewise blade bending moments for blades of this size.

Table 6-1. Summary of IEC DLC Settings

DLC	Wind Condition	Wind Speeds	Additional Settings	# of Seeds	# of Simulations
1.1	NTM	3:2:25 m/s	-	6	72
1.3	ETM	3:2:25 m/s	-	6	72
1.4	ECD	V_r, V_r±2 m/s	± Dir. Change	-	6
1.5	EWS	3:2:25 m/s	± Vert./Horz.	-	48
6.1	EWM	V_{50}	Yaw ±8°	6	12
6.3	EWM	V_1	Yaw ±20°	6	12

NTM	normal turbulence model
ETM	extreme turbulence model
ECD	extreme coherent gust with direction change
EWS	extreme wind shear
EWM	extreme wind speed model
$V_r = 10.8\,\mathrm{m/s}$	rated wind speed
$V_{50} = 50.0\,\mathrm{m/s}$	10-min average extreme wind speed with a 50-year return period
$V_1 = 40.0\,\mathrm{m/s}$	10-min average extreme wind speed with a 1-year return period

Table 6-2. Metocean Conditions Used in DLC Analysis

Operation	Wind Speed [m/s]	Significant Wave Height [m]	Peak Spectral Period [s]
Normal	4	1.102	8.515
	6	1.179	8.310
	8	1.316	8.006
	10	1.537	7.651
	12	1.836	7.441
	14	2.188	7.461
	16	2.598	7.643
	18	3.061	8.047
	20	3.617	8.521
	22	4.027	8.987
	24	4.516	9.452
Extreme 1-yr return	40	9.686	16.654
Extreme 50-yr return	50	11.307	18.505

m meters   m/s meters per second   s seconds

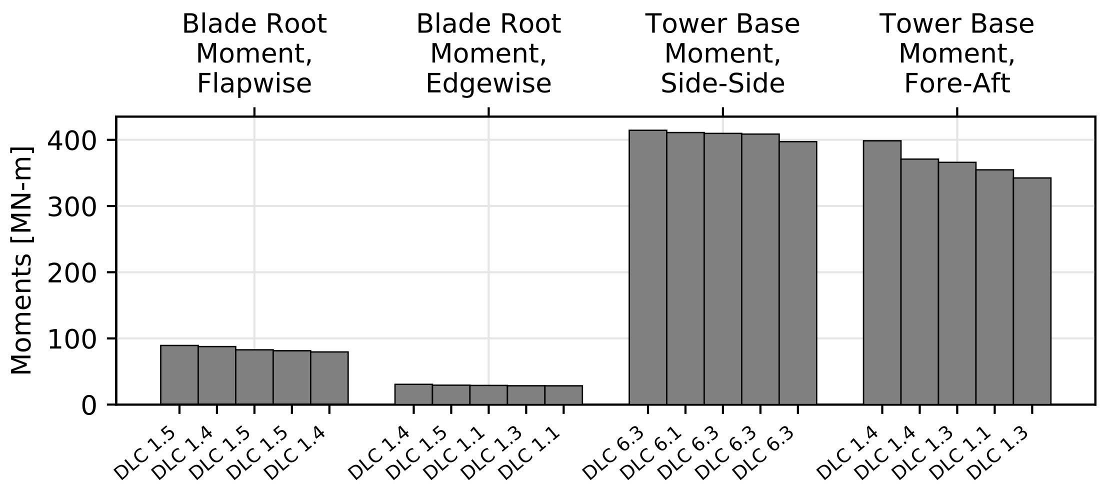

Figure 6-1. DLC ranking of maximum blade root and tower base bending moments

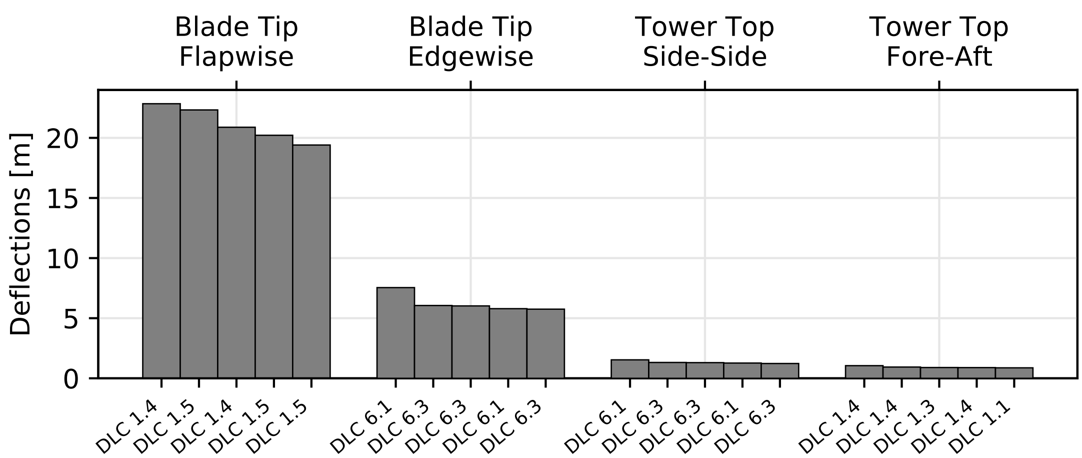

Figure 6-2. DLC ranking of maximum blade tip and tower top deflections

6.1 Conclusions

Publicly available reference wind turbine designs have proven to be an invaluable tool to the wind energy research community. As the technology has continued to mature and improve, subsequent reference turbines [2, 3, 5–9] have been developed to keep pace with, and ahead of, industry trends. In order to be relevant for forward-looking technology development and analysis efforts, reference wind turbines need to represent state-of-the-art or near-future wind turbine technology. This work was motivated by a gap in the available offshore reference turbine designs, between 10 MW and 20 MW, while the industry is moving beyond 10-MW designs.

This report documents the design and performance of the IEA Wind 15-MW reference wind turbine, jointly developed by NREL, DTU, and UMaine, in coordination with the second work package in IEA Wind Task 37 on Wind Energy Systems Engineering. This reference wind turbine represents a standardized design that can be used for concept studies as the industry progresses toward larger machines. It is a conventional three-bladed upwind design with a rotor diameter of 240 m; a 150-m hub height; a variable-speed, collective pitch controller; and a low-speed, direct-drive generator. A baseline steel monopile support structure is presented, which has been sized at a 30-m water depth. Subsequent work, in collaboration with UMaine, will document a floating support structure configuration on a steel semisubmersible.

Further details of the design, including OpenFAST, HAWC2, and WISDEM input files, are available at the IEA Wind Task 37 GitHub.

References

[1] WindEurope. *Offshore Wind in Europe. Key Trends and Statistics*. Tech. rep. WindEurope, 2019.

[2] Pietro Bortolotti, Helena Canet Tarrés, Katherine Dykes, Karl Merz, Latha Sethuraman, David Verelst, and Frederik Zahle. *IEA Wind TCP Task 37: Systems Engineering in Wind Energy - WP2.1 Reference Wind Turbines*. Tech. rep. International Energy Agency, 2019. DOI: 10.2172/1529216.

[3] INNWIND.EU. http://www.innwind.eu/publications/deliverable-reports. 2017.

[4] International Electrotechnical Commission. *Wind Turbines – Part 1: Design requirements*. Tech. rep. IEC 61400-1 Ed.3. 2005.

[5] G. Bywaters, V. John, J. Lynch, P. Mattila, G. Norton, J. Stowell, M. Salata, O. Labath, A. Chertok, and D. Hablania. *Northern Power Systems WindPACT Drive Train Alternative Design Study Report*. Tech. rep. 2004.

[6] J. Jonkman, S. Butterfield, W. Musial, and G. Scott. *Definition of a 5-MW Reference Wind Turbine for Offshore System Development*. Tech. rep. NREL/TP-500-38060. National Renewable Energy Laboratory, 2009.

[7] C. Bak, F. Zahle, R. Bitsche, and T. Kim. *Description of the DTU 10MW reference wind turbine*. Tech. rep. DTU Wind Energy Report I-0092. DTU Wind Energy, 2013.

[8] C. Desmond, J. Murphy, L. Blonk, and W. Haans. "Description of an 8 MW reference wind turbine." In: *Journal of Physics: Conference Series* (2016). DOI: 10.1088/1742-6596/753/9/092013.

[9] D. Griffith and T. Ashwill. *The Sandia 100-meter All-glass Baseline Wind Turbine Blade : SNL100-00*. Tech. rep. SAND2011-3779. Sandia National Laboratories, 2011.

[10] Katherine Dykes, Peter Graf, George Scott, Andrew Ning, Ryan King, Yi Guo, Taylor Parsons, Rick Damiani, Fort Felker, and Paul Veers. "Introducing WISDEM: An Integrated System Model of Wind Turbines and Plants." In: *Third Wind Energy Systems Engineering Workshop, January 14, 2015*. Boulder, CO, 2015.

[11] *WISDEM*. 2019. URL: https://github.com/WISDEM/WISDEM.

[12] "Aero-Elastic Optimization of a 10 MW Wind Turbine." English. In: *Proceedings - 33rd Wind Energy Symposium*. Vol. 1. American Institute of Aeronautics and Astronautics, 2015, pp. 201–223.

[13] "Design of an aeroelastically tailored 10 MW wind turbine rotor." English. In: vol. 753. IOP Publishing, 2016. DOI: 10.1088/1742-6596/753/6/062008.

[14] S. A. Ning. *CCBlade Documentation: Release 1.1.0*. Tech. rep. National Renewable Energy Laboratory (NREL), Golden, CO (United States), 2013. URL: http://wisdem.github.io/CCBlade/.

[15] SA Ning. *RotorSE Documentation: Release 0.1.0*. Tech. rep. National Renewable Energy Lab. (NREL), Golden, CO (United States), 2014. URL: http://wisdem.github.io/RotorSE/.

[16] Gunjit S. Bir. *User's Guide to PreComp*. Tech. rep. Golden, CO: National Renewable Energy Laboratory, 2005.

[17] José Pedro Albergaria Amaral Blasques. *User's Manual for BECAS: A cross section analysis tool for anisotropic and inhomogeneous beam sections of arbitrary geometry*. Tech. rep. 2012.

[18] G. Bir. *User's Guide to BModes*. Tech. rep. NREL/TP-500-39133. Golden, Colorado: National Renewable Energy Laboratory, 2005.

[19] Jason M. Jonkman and Marshall L. Buhl Jr. *FAST User's Guide*. Tech. rep. NREL/EL-500-38230. Golden, Colorado: National Renewable Energy Laboratory, 2005. DOI: 10.2172/15020796.

[20] *OpenFAST Documentation*. 2019. URL: https://openfast.readthedocs.io/en/master/.

[21] Torben J. Larsen and Anders Melchior Hansen. *How 2 HAWC2, the user's manual*. Tech. rep. 2007.

[22] M. Hansen, L. Henriksen, C. Tibaldi, L. Bergami, D. Verelst, G. Pirrung, and R. Riva. *HAWCStab2 User Manual*. Tech. rep. Roskildem, Denmark: Technical University of Denmark, 2018.

[23] Justin S. Gray, John T. Hwang, Joaquim R. R. A. Martins, Kenneth T. Moore, and Bret A. Naylor. "OpenMDAO: An open-source framework for multidisciplinary design, analysis, and optimization." In: *Structural and Multidisciplinary Optimization* 59.4 (Apr. 2019), pp. 1075–1104. DOI: 10.1007/s00158-019-02211-z.

[24] Gordon M. Stewart, Amy Robertson, Jason Jonkman, and Matthew A. Lackner. "The creation of a comprehensive metocean data set for offshore wind turbine simulations." In: *Wind Energy* 19.6 (2016), pp. 1151–1159. DOI: 10.1002/we.1881.

[25] Jess A Michelsen. *Basis3D-a platform for development of multiblock PDE solvers*. Tech. rep. AFM 92-05, Technical University of Denmark, 1992.

[26] Jess A Michelsen. "Block structured Multigrid solution of 2D and 3D elliptic PDE's." PhD thesis. 1994.

[27] Niels N. Sørensen. "General purpose flow solver applied to flow over hills." Published 2003. PhD thesis. 1995.

[28] Niels N. Sørensen. *HypGrid2D a 2-D mesh generator*. Tech. rep. 1035(EN). 1998.

[29] Florian Menter. "Zonal two equation kw turbulence models for aerodynamic flows." In: *23rd fluid dynamics, plasmadynamics, and lasers conference*, p. 2906.

[30] Mark Drela and Michael B Giles. "Viscous-inviscid analysis of transonic and low Reynolds number airfoils." In: *AIAA journal* 25.10 (1987), pp. 1347–1355.

[31] Zhaohui Du and Michael S. Selig. "A 3-D stall-delay model for horizontal axis wind turbine performance prediction." English (US). In: AIAA/ASME Wind Energy Symposium, 1998 ; Conference date: 12-01-1998 Through 15-01-1998. Jan. 1998, pp. 9–19.

[32] K. Dykes et al. *System Modeling Frameworks for Wind Turbines and Plants.* Tech. rep. In preparation. International Energy Agency.

[33] Yu Wenbin. *VABS Manual for Users*. Tech. rep. West Jordan, UT: AnalySwift, 2011.

[34] T. Pflumm, W. Garre, and M. Hajek. "A preprocessor for parametric composite rotor blade cross-sections." In: *44th European Rotocraft Forum*. Delft, The Netherlands, 2018.

[35] José Pedro Albergaria Amaral Blasques and Mathias Stolpe. "Multi-material topology optimization of laminated composite beam cross sections." In: *Composite Structures* 94.11 (2012), pp. 3278–3289. ISSN: 0263-8223. DOI: https://doi.org/10.1016/j.compstruct.2012.05.002.

[36] J. Rinker, E. Gaertner, P. Bortolotti, W. Skrzypinski, F. Zahle, H. Bredsmoe, G. Barter, and K. Dykes. "Comparison of loads from HAWC2 and FAST for the IEA 15 MW Reference Wind Turbine." In: *Torque 2020*.

[37] National Renewable Energy Laboratory. *ROSCO. Version 0.1.0*. 2019. URL: https://github.com/NREL/rosco.

[38] M. H. Hansen and L. C. Henriksen. *Basic DTU Wind Energy controller*. Tech. rep. DTU Wind Energy Report E-0018. DTU Wind Energy, 2013.

[39] N. J. Abbas, L. Pao, and A. Wright. "An Update to the National Renewable Energy Laboratory Wind Turbine Controller." In: *Journal of Physics: Conference Series* (). In preparation.

[40] Laszlo Arany, S. Bhattacharya, John Macdonald, and S. J. Hogan. "Design of monopiles for offshore wind turbines in 10 steps." In: *Soil Dynamics and Earthquake Engineering* 92 (2017), pp. 126–152. ISSN: 0267-7261. DOI: https://doi.org/10.1016/j.soildyn.2016.09.024. URL: http://www.sciencedirect.com/science/article/pii/S0267726116302937.

[41] Suresh C. Arya, Michael W. O'Neill, and George Pincus. *Design of structures and foundations for vibrating machines*. Gulf Pub Co, 1979.

[42] Johan N. Stander, Gerhard Venter, and Maarten J. Kamper. "Review of direct-drive radial flux wind turbine generator mechanical design." In: *Wind Energy* 15.3 (2012), pp. 459–472. DOI: 10.1002/we.484.

[43] E. Smith. "DESIGN AV NACELLE FOR EN 10 MW VINDTURBIN." MA thesis. Norwegian university of science and technology, 2012.

[44] Latha Sethuraman and Katherine Dykes. *GeneratorSE: A Sizing Tool for Variable-Speed Wind Turbine Generators*. Tech. rep. NREL/TP-5000-66462. National Renewable Energy Laboratory, 2017. URL: https://www.nrel.gov/docs/fy17osti/66462.pdf.

[45] Hung Vu Xuan. "Modeling of Exterior Rotor Permanent Magnet Machines with Concentrated Windings." PhD thesis. 2012.

[46] Ion Boldea. *Synchronous generators*. CRC Press, 2015.

[47] Alasdair Stewart McDonald. "Structural analysis of low speed, high torque electrical generators for direct drive renewable energy converters." PhD thesis. University of Edinburgh, 2008.

[48] P. C. J. Hoogenboom and R. Spaan. "Shear Stiffness and Maximum Shear Stress of Tubular Members." In: *Proceedings of the Fifteenth International Offshore and Polar Engineering Conference. International Society of Offshore and Polar Engineers*. (Jan. 1, 2005). ISOPE-I-05-399. Seoul, Korea, 2005.

A Blade Cross Sections

Renderings of the spanwise blade cross sections are shown in this section. The 70% spanwise location is shown in Figure 2-6.

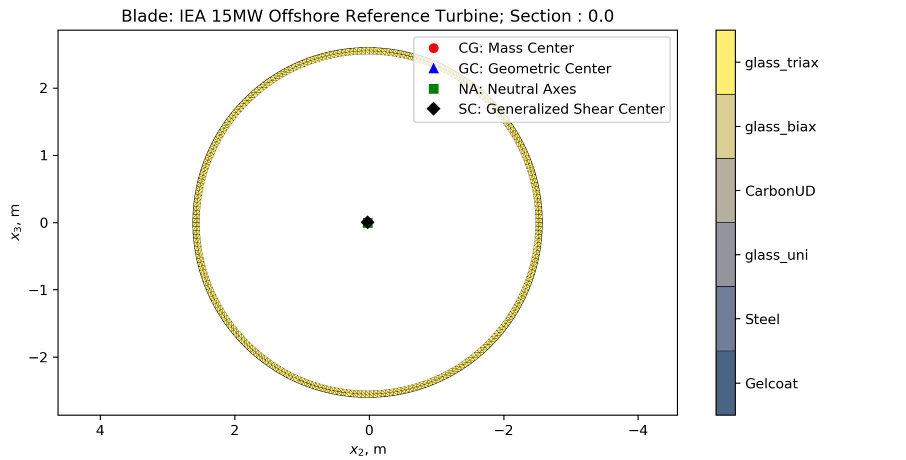

Figure A-1. Blade cross section at 0% span

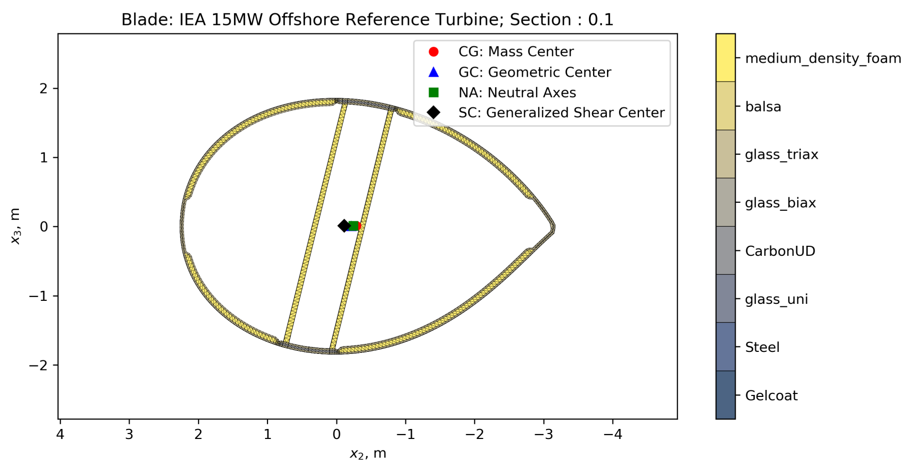

Figure A-2. Blade cross section at 10% span

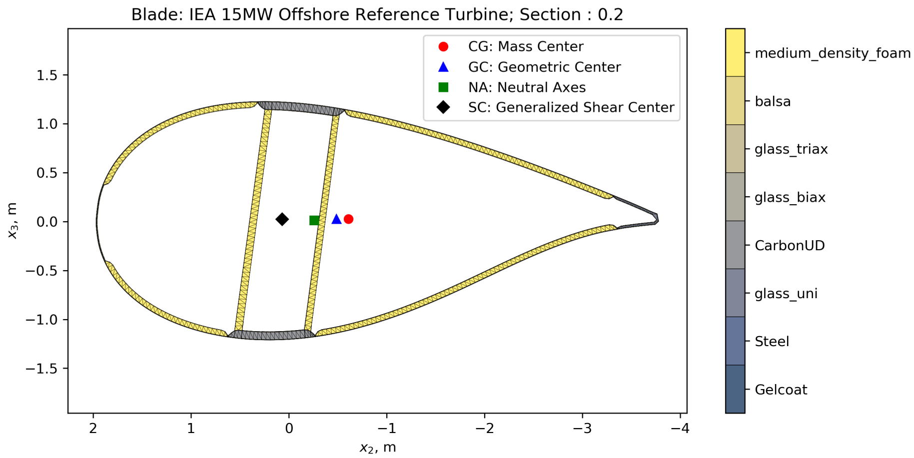

Figure A-3. Blade cross section at 20% span

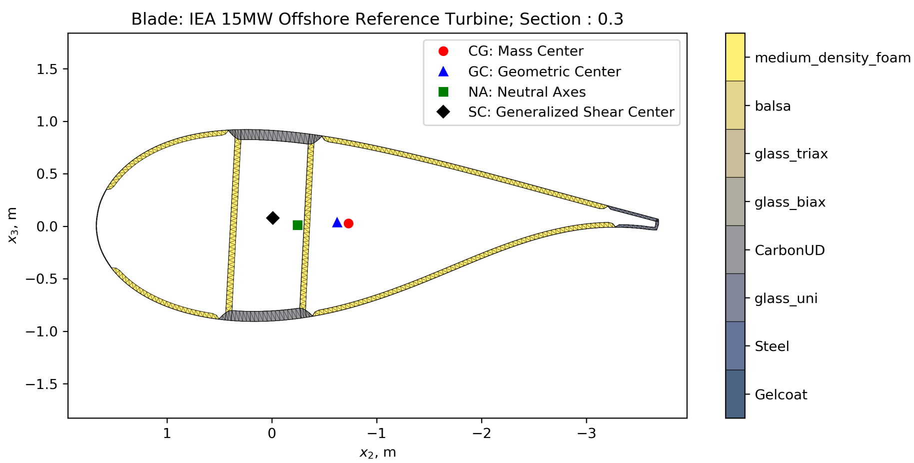

Figure A-4. Blade cross section at 30% span

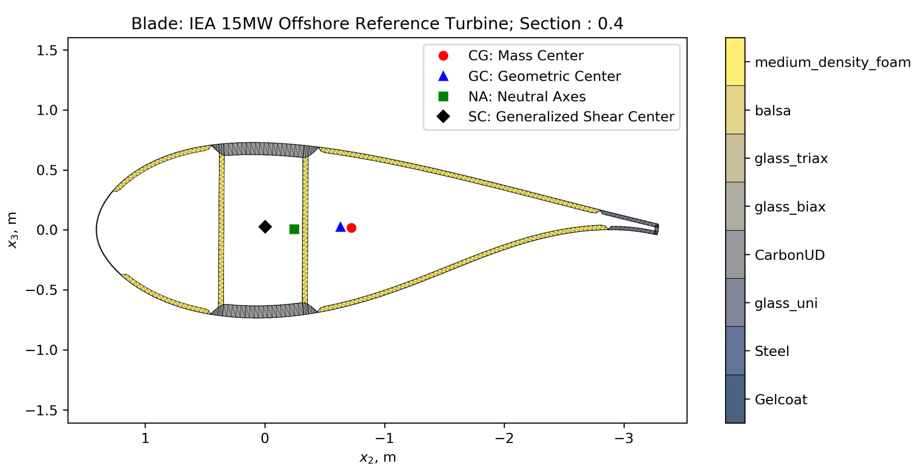

Figure A-5. Blade cross section at 40% span

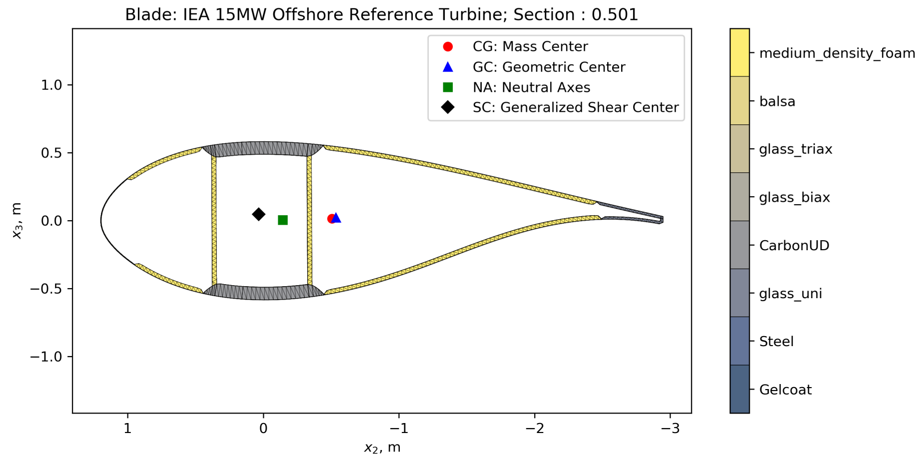

Figure A-6. Blade cross section at 50% span

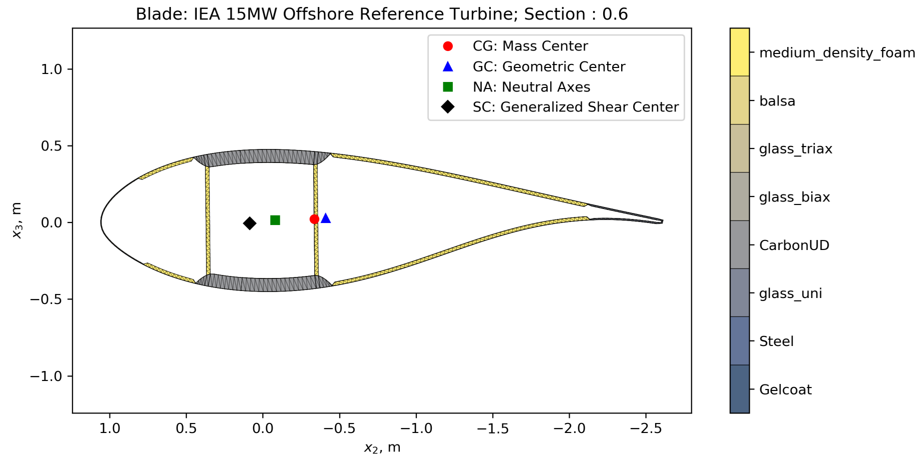

Figure A-7. Blade cross section at 60% span

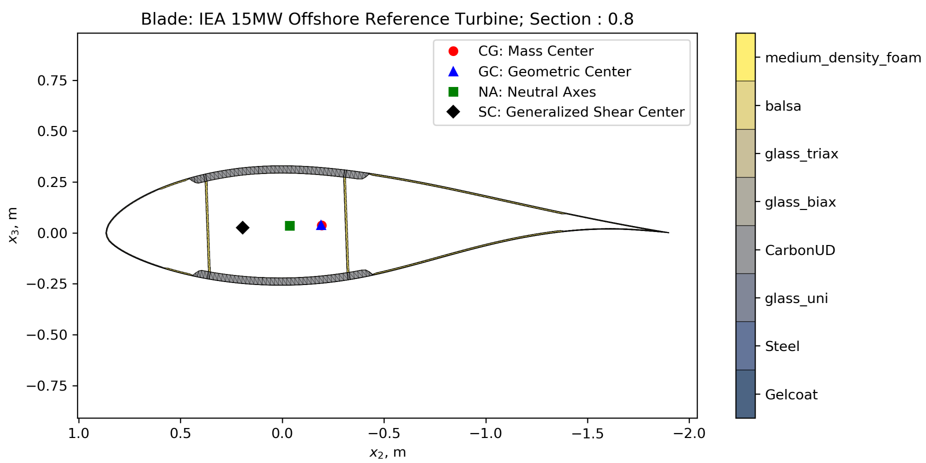

Figure A-8. Blade cross section at 80% span

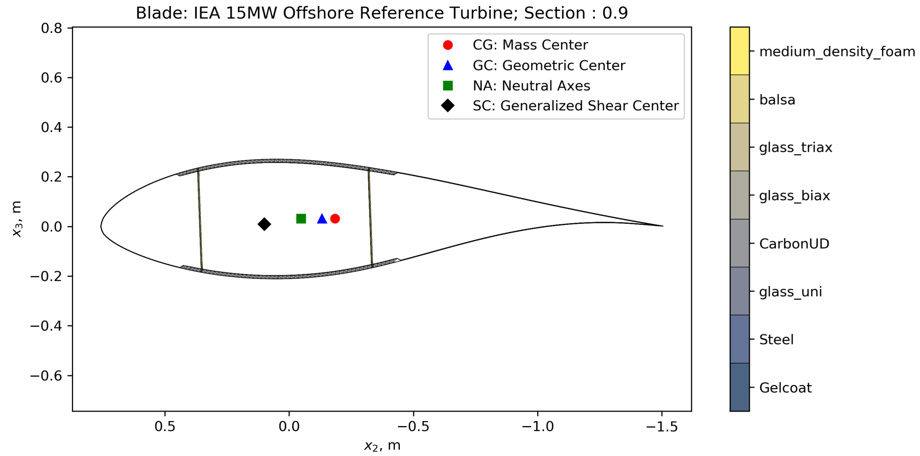

Figure A-9. Blade cross section at 90% span

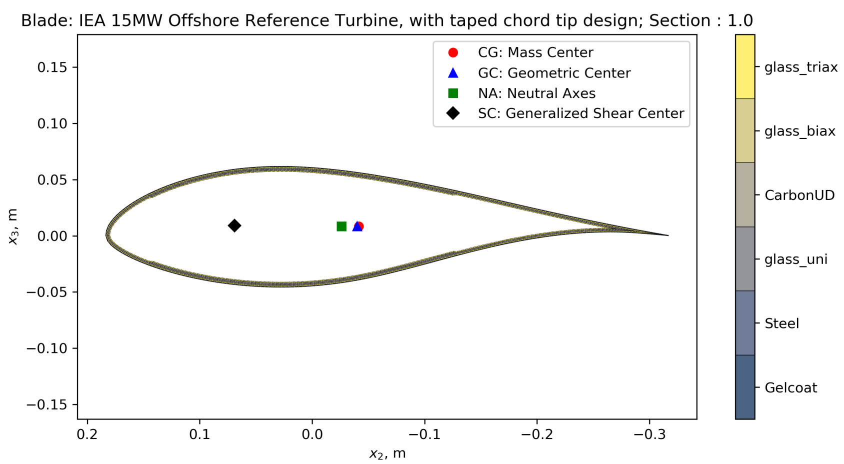

Figure A-10. Blade cross section at 100% span

B Tower and Soil Modeling

B.1 Tower Data

The equations used to calculate cross-sectional tower properties are provided in this section. The definitions of the terms used in Figure 4-3 are:

- Mass density is equal to m
- Flapwise inertia is equal to $m\,r_{ix}^2$
- Edgewise inertia is equal to $m\,r_{iy}^2$
- Flapwise stiffness is equal to EI_x
- Edgewise stiffness is equal to EI_y
- Torsional stiffness is equal to GK
- Axial stiffness is equal to EA.

B.1.1 Station, r [m]

The distance along the tower from the base. For the land-based HAWC2 model, this is assumed to start at 0 meters (m) and end at 145.0 m. Thus, the tower model includes the transition piece, which extends from 0 m to 15 m.

B.1.2 Mass per Unit Length, m [kg/m]

Mass per unit length of the tower:

$$m = \rho A \tag{B.1}$$

$$= \rho\,\pi\left[(D/2)^2 - (D/2-t)^2\right], \tag{B.2}$$

where A is the cross-sectional area, D is the outer diameter, and t is the wall thickness at a given station.

B.1.3 Center of Mass, x_m [m]

The x location of the center of mass. Because the tower is axisymmetric, this value is zero, $x_m = 0$.

B.1.4 Center of Mass, y_m [m]

The y location of the center of mass. Because the tower is axisymmetric, this value is zero, $y_m = 0$.

B.1.5 Radius of Gyration, r_{ix} [m]

The radius of gyration around the principal bending axis, x_e. We use the radius of gyration to calculate the mass moment of inertia for a cross section, which we need for inertia calculations. for an isotropic circular tube:

$$r_{ix} = \sqrt{\frac{I_x}{A}}, \tag{B.3}$$

$$= \sqrt{\frac{\pi\left[(D/2)^4 - (D/2-t)^4\right]/4}{\pi\left[(D/2)^2 - (D/2-t)^2\right]}}, \tag{B.4}$$

$$= \sqrt{\frac{1}{4}\left[(D/2)^2 + (D/2-t)^2\right]}. \tag{B.5}$$

B.1.6 Radius of Gyration, r_{iy} [m]

Radius of gyration around the principal bending axis, y_e, is the same as r_{ix} due to symmetry.

B.1.7 Shear Center, x_s [m]

The x-coordinate of the shear center. Because the cross section is symmetric about both x and y, the shear center is collocated with the elastic center (which is at the origin), $x_s = 0$.

B.1.8 Shear Center, y_s [m]

The y coordinate of the shear center. Because the cross section is symmetric about both x and y, the shear center is collocated with the elastic center (which is at the origin), $y_s = 0$.

B.1.9 Young's Modulus, E [Pa]

The Young's modulus with values in Table 4-1.

B.1.10 Shear Modulus, G [Pa]

The shear modulus with values in Table 4-1.

B.1.11 Area Moment of Inertia, I_x [m^4]

Area moment of inertia around the principal bending axis, x_e:

$$I_x = \int_A x^2 dxdy \tag{B.6}$$

$$= \frac{\pi}{4}\left[(D/2)^4 - (D/2 - t)^4\right] \tag{B.7}$$

B.1.12 Area Moment of Inertia, I_y [m^4]

Area moment of inertia around the principal bending axis, y_e:

$$I_y = \int_A y^2 dxdy \tag{B.8}$$

$$= \frac{\pi}{4}\left[(D/2)^4 - (D/2 - t)^4\right] \tag{B.9}$$

B.1.13 Torsional Stiffness Constant, K [m^4/rad]

Torsional stiffness constant calculated about the z axis at the shear center. Because we assume a circular section, this is equivalent to the polar moment of inertia:

$$K = \int_A r^2 dxdy, \tag{B.10}$$

$$= \frac{\pi}{2}\left[(D/2)^4 - (D/2 - t)^4\right]. \tag{B.11}$$

B.1.14 Shear Reduction Factor, k_x [-]

Shear factor, also called the shear reduction factor, for shear in the x direction. Per [48], we use the following shear factor:

$$k_x = \frac{1}{2} + \frac{3}{4}\frac{2t}{D}. \tag{B.12}$$

B.1.15 Shear Reduction Factor, k_y [-]

Shear factor, also called the shear reduction factor, for shear in the y direction. Per [48], we use the following shear factor:

$$k_y = \frac{1}{2} + \frac{3}{4}\frac{2t}{D}. \tag{B.13}$$

B.1.16 Cross-Sectional Area, A [m^2]

The area of the cross section:

$$A = \int_A dxdy, \tag{B.14}$$

$$= \pi\left[(D/2)^2 - (D/2-t)^2\right]. \tag{B.15}$$

B.1.17 Structural Pitch, θ_s [deg]

This is the angle between x and the principal bending axis most parallel to x. Because the tower is axisymmetric, this is zero, $\theta_s = 0$).

B.1.18 Elastic Center, x_e [m]

The x location of the elastic center, which is the intersection point for the principal bending axes. Because the tower is axisymmetric about z, this is 0, $x_e = 0$.

B.1.19 Elastic Center, y_e [m]

The y location of the elastic center. Because the tower is axisymmetric about z, this is 0, $y_e = 0$.

B.2 Soil Model

B.2.1 Vertical Stiffness

Stiffness of the soil in the vertical direction for circular structures. This is sometimes ignored because monopiles and towers are relatively stiff in their axial directions:

$$\eta_z = 1 + 0.6\,(1-\nu)\,\frac{h}{r_0} \tag{B.16}$$

$$k_z = \frac{4Gr_0}{1-\nu}\eta_z \tag{B.17}$$

B.2.2 Horizontal Stiffness

Stiffness of the soil in the lateral direction for circular structures:

$$\eta_x = 1 + 0.55\,(2-\nu)\,\frac{h}{r_0} \tag{B.18}$$

$$k_x = \frac{32\,(1-\nu)\,Gr_0}{7-8\nu}\eta_z \tag{B.19}$$

B.2.3 Rocking Stiffness

Stiffness of the soil in the rocking direction for circular structures:

$$\eta_\psi = 1 + 1.2\,(1-\nu)\,\frac{h}{r_0} + 0.2\,(2-\nu)\left(\frac{h}{r_0}\right)^3 \tag{B.20}$$

$$k_\psi = \frac{8Gr_0^3}{3\,(1-\nu)}\eta_\psi \tag{B.21}$$

B.2.4 Torsional Stiffness

Stiffness of the soil in the rocking direction for circular structures:

$$k_\phi = \frac{16Gr_0^3}{3} \tag{B.22}$$